https://doi.org/10.1016/j.scp.2022.100749

From agricultural wastes to a resource: Kiwi Peels, as long-lasting, recyclable adsorbent, to remove emerging pollutants from water. The case of Ciprofloxacin removal.

Jennifer Gubitosa[a], Vito Rizzi[a]*, Domenico Cignolo[a], Paola Fini[b], Fiorenza Fanelli[c], Pinalysa Cosma[a]*

[a]Università degli Studi "Aldo Moro" di Bari, Dipartimento di Chimica, Via Orabona, 4- 70126 Bari, Italy;
[b]Consiglio Nazionale delle Ricerche CNR-IPCF, UOS Bari, Via Orabona, 4- 70126 Bari, Italy;
[c]Consiglio Nazionale delle Ricerche, Istituto di Nanotecnologia (CNR-NANOTEC) c/o Dipartimento di Chimica, Università degli Studi "Aldo Moro", Via Orabona, 4 - 70126 Bari, Italy.

Dr. Jennifer Gubitosa and Vito Rizzi contributed equally to the paper development.

*Prof. Pinalysa COSMA and Dr. Vito RIZZI
Università degli Studi "Aldo Moro" di Bari
Dipartimento di Chimica
Via Orabona, 4
I-70126 Bari, ITALY
e-mail: pinalysa.cosma@uniba.it

vito.rizzi@uniba.it
tel. +39 0805443443

ABSTRACT

This work accounts for the first example of dry Kiwi Peels to remove emerging pollutants from water. Both the inner and outer sides of Kiwi Peels were characterized by using in synergy FTIR-ATR, TG, and SEM analyses before and after its use and re-use, proposing it as long-lasting, recyclable adsorbent material. Among the tested 14 emerging pollutants, 6 of them were successfully removed by Kiwi Peels, also if present in mixtures, calculating the Kiwi Peels maximum adsorption capacities, occurring in the range of 1-4 mg/g. To infer information about the behavior of Kiwi Peels during water treatments, Ciprofloxacin, a well-known and largely used antibiotic, was selected as a dangerous model contaminant. The roles of ionic strength, pH values, adsorbent/pollutant amounts, and temperature values during the adsorption process were assessed, giving physical and chemical information about the whole adsorption process. The thermodynamics, the adsorption isotherms, and kinetics were studied. The Freundlich model, with a good correlation, well described the obtained results, indicating the heterogenous character of the Ciprofloxacin adsorption with the formation of a multilayer of pollutant molecules onto the adsorbent surface. If, on the one hand, in the range of temperatures 283-303K, the Ciprofloxacin adsorption was favored by increasing the temperature, on the other hand, the adsorption was hindered by further incrementing of temperature due to the pollutant desorption. Until the occurrence of desorption, the process occurred with $\Delta H° > 0$ and $\Delta S° > 0$ with a $\Delta G° < 0$. Both the pseudo-first and pseudo-second-order kinetic equations seemed to describe the process with the applicability of the Weber-Morris model. The results suggested the main presence of electrostatic interaction between the pollutant and adsorbent by changing the pH values and ionic strength of

Ciprofloxacin solutions. As a whole, from the obtained results, the best condition to remove Ciprofloxacin is neutral pH in the absence of salt at 303K. The Kiwi Peels and Ciprofloxacin recycling was also investigated by performing desorption experiments using 0.1M $MgCl_2$ solution, increasing the Kiwi Peels maximum adsorption capacity at least from 4 to 40 mg/g for Ciprofloxacin. At least 10 cycles of adsorption/desorption were performed, desorbing almost 75% of adsorbed pollutants during each run. Preliminary information about the possibility of inducing the solid-state pollutant photodegradation by using Advanced Oxidation Processes was also explored, giving a possible alternative for pollutant desorption and adsorbent recycling.

KEYWORDS: Kiwi Peels; Emerging pollutants; Ciprofloxacin; Adsorption; Recycling; Photodegradation.

1. INTRODUCTION

Several components usually pollute wastewater and water matrices also as a mixture of various contaminants, such as heavy metals, inorganic salts, and textile dyes, with high toxicity (Obinna and Ebere, 2019). So, suitable strategies, especially devoted to adsorption techniques, to obtain clean water were carefully developed and well described in the recent and past literature (Iwuozor et al., 2022; Rashed, 2013; Rigoletto et al., 2022; Rizzi et al., 2018, 2017).

However, as a relatively rising and global problem, Emerging Pollutants (EPs) are increasingly present. These are not regulated substances that could affect human health and the whole environment, inducing severe problems as already reported in our previous works (Rizzi et al., 2021, 2020b, 2020a, 2019a). Personal care products, pharmaceutical industry wastes, hospitals, and agricultural wastewater are examples of samples containing EPs that could affect water quality (Azizi, 2021). Different approaches were investigated to solve this problem(Liakos et al., 2021). However, due to the economic aspects and possible dangerous secondary by-products, most reported approaches are not easily applicable (Afolabi et al., 2020). On the other hand, due to the usually associated low costs and simplicity, the adsorption process was largely employed to treat water according to Green Chemistry and Sustainable Development principles (Rizzi et al., 2021). For example, to remove pharmaceutical compounds and textile dyes, natural biopolymers (*i.e.*, chitosan, alginate) and agricultural wastes have gained great interest in the last years under the circular economy philosophy (Rizzi et al., 2020a, 2019a, 2017). The Bhatnagar *et al*.(Bhatnagar et al., 2015) review is very explicative by presenting Peels from fruits and vegetables employable as precursors to obtain activated carbon for water remediation. Although most of the Peels from fruits were largely investigated (Aman et al., 2008; Shuaibing and Qihua, 2013; Xu et al., 2014), Kiwi Peels present only few applications, suggesting that the Kiwi Fruit by-products could be furtherly valorized, giving these wastes the possibility to become a resource (Sanz et al., 2021).

Indeed, Chamorro *et al*. reported that in 2019, Kiwi cultivation occupied a surface of ~ 270 × 103 ha worldwide, and Europe contributed with ~ 43 × 103 ha. Accordingly, the Kiwi waste production is high, and it accounts globally for ~ 4.5 × 106 tons, whereas Europe produces ~1 × 106 tons (Chamorro et al., 2022). Consequently, this implies a huge global production of Kiwi wastes with dangerous consequences for the environment, encouraging the use of circular economy approaches as the most pertinent. Therefore, the latter should be supported for more sustainable development. To our knowledge, in the available literature, the Kiwi's cortex use was described to remove Cd^{2+}, Cr^{3+} and Zn^{2+} ions (Al-Qahtani, 2016), nitrate (Mokif et al., 2018), and oil (Saleh Jafer and Hassan, 2019), or to obtain activated carbon for the removal of Pb^{2+} (Rahimnejad et al., 2018). While it is worth noting that the use of Kiwi Peels to remove organic pollutants, such as EPs, from water is not discussed.

On this ground, the present work aims to widen the Kiwi Peels' applicability by proposing them as an adsorbent to remove EPs from water by adopting safe work conditions, reducing the environmental impact and the associated costs. Indeed, only a few washing cycles with water were used as Kiwi Peels' pretreatment to remove the pulp and dirty present on them. Propoxur, Atenolol, Carbendazim, Furosemide, Ciprofloxacin (CIP), Paracetamol, Tetracycline (TC), Sulfamethoxazole, Carbamazepine, Diclofenac (DCF), Ketoprofen (Kp), Naproxen, Propranolol (PRO), and Hydrochlorothiazide (HCTZ) were tested as EPs. CIP, PRO, TC, DCF, Kp, and HCTZ were successfully removed, evidencing Kiwi Peels' potential concerning other adsorbents that remove few pollutants. Among the various tested EPs, the attention was focused on the antibiotics class, largely used to treat different diseases, because it is well-known how their improper disposal worsens the water contamination problem (Nassar et al., 2019), becoming a worldwide concern for the last few decades (Afzal et al., 2018; Gothwal and Shashidhar, 2015; Ulyankina et al., 2021). In addition, among the most used antibiotics, the Ciprofloxacin was selected as a model pollutant due to its well-known negative environmental impact (Ashiq et al., 2019; Fan et al., 2020; Khan et al., 2020; Ma et al., 2015; Tran et al., 2019; Yu et al., 2018). This choice was due to the current use of

fluoroquinolones antibiotics, including Ciprofloxacin, for treating patients affected by SARS-CoV-2 associated pneumonia, whose massive use could increase water pollution, also considering that, unfortunately, about 80% of the CIP's consumed amount is excreted unaltered into the effluents (Eze et al., 2021; Ji et al., 2021; Ulyankina et al., 2021). The importance and relevance to the CIP's removal are evident by looking at the very high number of works available in the literature and reported in **Table 1** (and references therein) (Afzal et al., 2018; Ashiq et al., 2019; Azizi, 2021; Balarak et al., 2021a, 2021b; Eze et al., 2021; Fu et al., 2021; Gao et al., 2021; Hao et al., 2021; Ji et al., 2021; Khan et al., 2020; Li et al., 2021, 2017; Lu et al., 2020; Ma et al., 2021; Mohammadi Nodeh et al., 2018; Peñafiel et al., 2021; Rizzi et al., 2021; Wang et al., 2020; Yu et al., 2018; Zhang et al., 2019; Zhao et al., 2017; Zheng et al., 2020).

Table 1: Some of the recent articles for the removal of CIP from water

Adsorbent	**Maximum adsorption capacity Q_{max} mg/g**	**Reference**
***Azolla filiculoides* activated carbon**	35.14	Balarak *et al.* 2021 (a)
Synthesized NiO	84.72-87.9	Balarak *et al.* 2021 (b)
Tannin foam immobilized with ferric ions	91.8	Hao *et al.* 2021 (Hao et al., 2021)
Acid Enhanced *Dialium guineense* Seed Waste	125	Eze *et al.* 2020 (Eze et al., 2021)

Sugarcane bagasse from Ecuador	13.6	Peñafiel *et al.* 2021 (Peñafiel et al., 2021)
Lignin-based adsorbents	0.2-0.4	Gao *et al.*2021 (Gao et al., 2021)
Titanate nanotubes	153.90	Ji *et al.*2021 (Ji et al., 2021)
Adsorbent from sludge pyrochar	10.42	Li *et al.* 2021 (Li et al., 2021)
Magnetic sludge biochar	74.2	Ma *et al.*2021 (Ma et al., 2021)
Cyclodextrin Nanosponges	2	Rizzi *et al.* 2021 (Rizzi et al., 2021b)
Iron oxide/cellulose magnetic recyclable nanocomposite	168.03	Azizi *et al.*2021 (Azizi, 2021)
Nanocomposite beads	9.21-10.87	Wang *et al.* 2020 (Wang et al., 2020)
Graphene oxide-based adsorbent	1826.64	Khan *et al*. 2020 (Khan et al., 2020)
Diamine-functionalized MCM-41	139.25	Lu *et al.* 2020 (Lu et al., 2020)

Magnetic biosorbents	527.93	Zheng *et al.* 2020 (Zheng et al., 2020)
Municipal solid waste biochar-montmorillonite composite	167.36	Ashiq *et al.* 2019 (Ashiq et al., 2019)
Sulfate-reducing bacteria sludge	7.642	Zhang *et al.* 2019 (Zhang et al., 2019)
Modified waste grapefruit peel	565	Fu *et al.*2019 (Fu et al., 2021)
Polyaniline-magnetic graphene oxide nanocomposite	106.38	Nodeh *et al.* 2018 (Mohammadi Nodeh et al., 2018)
Ethylene diaminetetraacetic acid– β -cyclodextrin	448	Yu *et al.* 2018 (Yu et al., 2018)
Chitosan hydrogel beads	1.024	Afzal *et al.* 2018 (Afzal et al., 2018)
Nanoporous carbon from Zeolitic imidazolate framework-8	416.7	Li *et al.* 2017 (Li et al., 2017)
chitosan-EDTA-β-cyclodextrin polymer	47	Zhao *et al.* 2017 (Zhao et al., 2017)
Kiwi Peels	**40**	**This work**

125

The selected papers were chosen as examples for comparing with this paper, evidencing the very different nature of adopted approaches and the obtained different adsorption capacities that changes from a few to some thousands of mg/g. Among articles reported in **Table 1**, only some of them propose the adsorbent regeneration and thus the CIP desorption. Moreover, the adsorbent recycling was obtained through not safe and not environmentally friendly technologies, except for the work of Rizzi *et al.*(Rizzi et al., 2021). Particularly, by adopting Tannin foam immobilized with ferric ions, Hao et al. (Hao et al., 2021) proposed the adsorbent recycling, for 5 cycles, by using 0.1M HCl. However, regeneration into an iron solution was necessary after each cycle (Hao et al., 2021). Again, the use of HCl to desorb CIP was reported during the employment of Dialium guineense seed waste (Eze et al., 2021) and iron oxide/cellulose magnetic nanocomposites (Azizi, 2021). Additionally, magnetic bio sorbents (Zheng et al., 2020) and a graphene oxide-based material (Khan et al., 2020) desorbed CIP using HCl or a mixture of ethanol/HCl. Titanate nanotubes were regenerated in deionized water, obtaining a very low % of CIP desorption (Ji et al., 2021). An adsorbent from sludge pyrochar was recovered at a very high temperature, i.e., 450°C (Li et al., 2021). The co-processing of ultrasound and ethanol was suggested as a suitable method to regenerate magnetic sludge biochar (Ma et al., 2021). Once again, using ultrasound, but in the presence of methanol (containing 10% ammonia), the zeolitic imidazolate framework-8 derived nanoporous carbon was recycled (Li et al., 2017). Diamine-functionalized MCM-41 was regenerated by using a very acidic solution (pH 3), and the same result was obtained with NaCl solution (3M) (Lu et al., 2020). Finally, methanol was adopted for the CIP desorption from nanocomposite of polyaniline and magnetic graphene oxide (Mohammadi Nodeh et al., 2018). Although these works reported high qmax values, the presented and investigated technologies generally don’t appear environmentally friendly. On the other hand, this work proposes the approach already adopted by Rizzi et al. (Rizzi et al., 2021), recycling the adsorbent by using “green” salts solutions. In this way, by performing at least 10 cycles of CIP’s adsorption and

desorption, potentially the Kiwi Peels' low adsorption capacity increased by rising from 4 to 40 mg/g, recycling both the pollutant and the adsorbent.

According to the circular economy principles, the proposed green approach is crucial in extending the adsorbent lifetime, being the main challenge for researchers working in this field (Rizzi et al., 2021, 2019a). Moreover, Kiwi Peels were also studied to remove other pollutants and mixtures (containing 2, 3, and 6 EPs), evidencing their good performances. So, novel horizons are opened in the field of EPs removal by adopting Kiwi Peels' wastes, and this paper represents the starting point for studies in which the Peels could be adopted by changing the strategies of their use. Work is in progress in our laboratory for widening the Kiwi Peels applicability for removing textile dyes, mixtures of dyes and EPs, and heavy metals. The ultimate goal will be the use under real conditions. At the moment, preliminary in-flux experiments have been performed and presented in this paper for the next future large-scale application.

Another aspect investigated in this work regards the possibility of using Advance Oxidation Processes (AOPs) to induce the CIP solid-state photodegradation as an alternative approach for adsorbent regeneration.

2. MATERIALS AND METHODS

2.1 Materials.

The used fruits were received, as wastes, from local providers located in Bari, South of Italy.

The following reagents were used and purchased form Sigma Aldrich, Milan, Italy: Ciprofloxacin ($C_{17}H_{18}FN_3O_3$, M.W. 331.35 g×mol^{-1}), ≥ 98,0%, (HPLC) and other tested pollutants; NaCl anhydrous, Redi-DriTM, ACS Reagent, ≥ 99%; NaOH, reagent grade, ≥ 98%, pellets (anhydrous); NaBr, BioXtra, ≥ 99%; KCl, Bio Reagent, suitable for cell culture, suitable for insect cell culture, ≥ 99%,; $CaCl_2$ anhydrous, granular, ≤ 7.0 mm, ≥ 93.0%; LiCl, Pure Reagent, RPE-ACS; NaI, ACS

Reagent, ≥ 99,5%; $NaClO_4$, ACS Reagent, ≥ 98.0%; $MgCl_2$, BioXtra, ≥ 99%,; HCl, ACS reagent, 37%.

The aqueous CIP stock solution (20 mg/L) was diluted at the following concentrations: 15, 10, 5, and 2.5 mg/L.

2.2 Adsorbent preparation.

The fruit peels were immersed in hot water until the fruit pulp was almost all removed. Particularly, 20 g of Peels were washed with 800 mL of hot water at 353 K and stirred for 15 minutes. Subsequently, the water was substituted, continuing the process until clean water was obtained (8 washing cycles are necessary). Finally, the thus produced Peels were dried until constant weight, obtaining the used dry adsorbent (see **Figure 3**). ≈ 50 € is the supposed cost to prepare 1 Kg of adsorbent.

2.3 UV-Visible measurements. A CARY 5 UV-Vis-NIR spectrophotometer (Varian Inc., now Agilent Technologies Inc., Santa Clara, CA, USA) was used to collect the UV-Vis absorption spectra in a range of 200–500 nm at a 1 nm/s scan rate. The Ciprofloxacin concentration was calculated by measuring the absorbance intensity at λ=335 nm, using the molar absorption coefficient (ε) of 14200 $L \times mol^{-1} \times cm^{-1}$ experimentally estimated by applying the Lambert-Beer law.

2.4 FTIR-ATR spectroscopy measurements. FTIR-ATR spectra of inner and outer Kiwi Peels surfaces before and after the pollutant adsorption/desorption were recorded in a 500–4000 cm^{-1} range by using a Fourier Transform Infrared spectrometer (FTIR Spectrum Two from Perkin Elmer, Waltham, MA, USA). The resolution was 4 cm^{-1}, and 16 scans were performed and summed for each acquisition.

2.5 Scanning Electron Microscopy (SEM) analyses. The morphology of the samples was investigated using a Zeiss SUPRA™ 40 Field Emission Scanning Electron Microscope (FE-SEM). All samples were coated with a thin layer of chromium (20 nm) before SEM observation. SEM images were acquired at electron acceleration voltage of 3 kV using a conventional Everhart-Thornley detector (working distance = 8-9 mm, magnification = 1-100 k×).

2.6 Thermal gravimetric (TG) analyses. The thermal investigation was carried out using TG (Perkin Elmer Pyris 1) analyses under an inert atmosphere using nitrogen as a purge gas, with a constant flow rate of 50 mL/min. Each sample (4-5 mg) was heated from 50°C to 700°C at a heating rate of 20 °C/min.

2.7 Gas-volumetric analysis. Nitrogen adsorption–desorption isotherms were measured at 77 K using a Micromeritics ASAP2010 volumetric sorption analyzer (Norcross, GA, USA). Before the adsorption measurements, the sample was outgassed at 80 °C under vacuum for 15 h to remove the adsorbates and residual moisture. The pore volumes and specific surface area, estimated using the BET equation, were inferred.

2.8 *In batch* equilibrium experiments. The Kiwi Peels adsorption capacities, q_t (mg×g^{-1}), for all the adsorbed pollutants were calculated by using **Equation 1** (Rizzi et al., 2021, 2020a):

$$q_t = \frac{C_0 - C_t}{W} \times V \qquad \textbf{(1)}$$

In the case of Ciprofloxacin, a systematic study was performed, and the values were also calculated at different contact times, *t*. *V* represents the pollutant solution volume (15 mL), *W* is the dried adsorbent mass (g), C_0 and C_t (mg/L) are the pollutant amounts at t_0 and *t* time, respectively. The % of adsorption (% of Ads) was calculated by using **Equation 2**:

$$\% \text{ of Ads} = \frac{A_0 - A_t}{A_0} \times 100 \quad \textbf{(2)}$$

A_0 and A_t are the UV-Vis absorbance intensities at λ=335 nm of a Ciprofloxacin solution measured at t_0 and t time.

During this work, to assess the pollutant amount role in the adsorption process, 25 mg of Kiwi Peels were placed into 15 mL of a Ciprofloxacin solution having different initial concentrations (from 20 mg/L to 2.5 mg/L) at pH 7.5. While the adsorbent amount role was investigated by changing the Kiwi Peels quantity from 12.5 to 80 mg in the presence of Ciprofloxacin at a constant concentration of 10 mg/L. The process was studied under continuous stirring. More information was gained by performing adsorption experiments in the presence of 25 mg of Kiwi Peels and 10 mg/L of Ciprofloxacin by changing the solution ionic strength with different salts at different concentrations. The pH (from 2 to 12) and temperature (from 283 to 323K) roles in the adsorption process were also investigated by holding the latter work conditions.

2.9 Adsorption kinetics. The kinetic information was obtained by applying the pseudo-first-order (PFO) and pseudo-second-order (PSO) kinetics models. **Equation 3** and **Equation 4** were used for PFO and PSO models, respectively (Fu et al., 2021; Gao et al., 2021; Hao et al., 2021; Ji et al., 2021; Li et al., 2021, 2017; Lu et al., 2020; Ma et al., 2021; Mohammadi Nodeh et al., 2018; Peñafiel et al., 2021; Rizzi et al., 2021, 2020a; Wang et al., 2020; Zhang et al., 2019; Zhao et al., 2017; Zheng et al., 2020).

$$\ln(q_e - q_t) = \ln(q_e) - K_1 \times t \quad \textbf{(3)}$$

$$\frac{t}{q_t} = \frac{1}{K_2 q_e^2} + \frac{1}{q_e} \times t \quad \textbf{(4)}$$

q_e (mg/L) represents the Kiwi Peels adsorption capacities at equilibrium, and q_t (mg/L) is the adsorption capacity at time t. k_1 (min^{-1}) and k_2 (g/(mg×min)) are the rate constants of PFO and PSO models, respectively.

The well-known **Equation 5** was also adopted to apply the intraparticle diffusion model described by the Weber-Morris equation (Rizzi et al., 2021).

$$q_t = k_{int} \times t^{1/2} + C \quad \textbf{(5)}$$

k_{int} represents the kinetic constant expressed in mg/(g×min$^{1/2}$), correlated to the intra-particle diffusion rate, and C is the thickness of the boundary layer.

2.10 Thermodynamic studies. Free energy ($\Delta G°$), entropy ($\Delta S°$), and enthalpy ($\Delta H°$) were evaluated for the Ciprofloxacin adsorption onto Kiwi Peels. For this purpose, different temperature values were adopted (ranging from 283 to 303K). Higher temperatures, although explored, did not favor the adsorption enabling the desorption instead (Rizzi et al., 2019a).

Equation 6 was used to calculate the free energy (Hao et al., 2021; Ma et al., 2015; Peñafiel et al., 2021):

$$\Delta G° = - RT \ln K_{eq} \quad \textbf{(6)}$$

R is the universal gas constant, 8.314 J×mol^{-1}×K^{-1}, T is the temperature (K), and K_{eq} represents the equilibrium constant expressed as q_e/C_e. The values of $\Delta H°$ and $\Delta S°$ were calculated by using Van't Hoff's equation (**Equations 7**):

$$\ln K_{eq} = -\frac{\Delta H^0}{RT} + \frac{\Delta S^0}{R} \quad \textbf{(7)}$$

2.11 Adsorption Isotherms. Langmuir, Freundlich, Temkin and Dubinin–Radushkevich models were used (Hao et al., 2021; Ji et al., 2021; Rizzi et al., 2021). In particular, when the isotherms functions fit well the experimental data, they can provide detailed and interesting information about the adsorption process. In particular, the Langmuir model considers that all the adsorption sites are characterized by constant energy. Furthermore, according to the model, a pollutant monolayer is adsorbed on the surface of the adsorbent materials with the absence of interactions between its molecules. **Equation 8** was used to represent the Langmuir model.

$$\frac{C_e}{q_e} = \frac{1}{K_L\, Q_0} + \frac{C_e}{Q_0} \quad \textbf{(8)}$$

Here q_e (mg/g) is the pollutant adsorbed amount at equilibrium, C_e is the correspondent equilibrium concentration in solution expressed in mg/L, K_L represents the Langmuir equilibrium constant (L/mg), and Q_0 is the adsorbent maximum adsorption capacity (mg/g) value.

On the other hand, the Freundlich isotherm model describes the adsorption onto a heterogeneous surface with adsorption sites having different energies as a function of the surface pollutant coverage. The heat of adsorption decreases exponentially during the process. **Equation 9** represents the Freundlich model.

$$\log(q_e) = \log(K_F) + \frac{1}{n}\log(C_e) \quad \textbf{(9)}$$

K_F ((mg/g)/(L/mg)$^{1/n}$) is the Freundlich constant and n is the heterogeneity factor. In particular, the 1/n value measures if the adsorption process is irreversible (1/n=0), favorable (0<1/n<1), or unfavorable (1/n>1).

The Temkin model accounts for the influence of the adsorbate-adsorbent interactions on the adsorption energy. Compared with the Freundlich model, the Temkin isotherm indicates that, during the adsorption process, the heat of adsorption decreases linearly during the process due to adsorbent/adsorbate interactions. **Equation 10** was used for the Temkin model.

$$q_e = B_1 \ln(K_T) + B_1 \ln(C_e) \quad \textbf{(10)}$$

K_T (L/mol) represents the equilibrium binding constant, and B_1 refers to the heat of adsorption.

Finally, the model of Dubinin–Radushkevich isotherm (D-R) was also applied. The model describes the adsorption onto a heterogeneous surface using a Gaussian energy distribution. **Equation 11** was applied to fit the experimental data.

$$\ln q_e = \ln(Q_0) - K_{D-R} \times \varepsilon^2 \quad \textbf{(11)}$$

295 q_e (mg/g) is the equilibrium adsorption capacity, Q_0 (mg/g) is the theoretical maximum adsorption
296 capacity, and $K_{D\text{-}R}$ (mol^2/J^2) is the Dubinin–Radushkevich isotherm constant. ε is the potential of
297 Polanyi, and it is described by **Equation 12**.

298 $$\varepsilon = RTln(1 + \frac{1}{C_e}) \quad \textbf{(12)}$$

299 with R = gas constant (8.314 J/mol K), T is the absolute temperature (K), and C_e represents the
300 pollutant equilibrium concentration (mg/L).
301 The model distinguishes between physical and chemical adsorption by inferring the value of energy,
302 E, calculated by applying **Equation 13**.

303 $$E = \frac{1}{\sqrt{2K_{D-R}}} \quad \textbf{(13)}$$

304 A value of E within the range 8-16 kJ/mol indicates that chemisorption is also present during the
305 adsorption process. While for E < 8 kJ/mol, the physisorption should be mainly considered (Azizi,
306 2021; Hao et al., 2021; Ji et al., 2021; Rizzi et al., 2021).
307
308 **2.12 *In batch* desorption experiments**. Experiments of desorption were executed both in hot water
309 and in the presence of different salt solutions at different concentrations. 0.1 M $MgCl_2$ was selected
310 to perform 10 cycles of adsorption and desorption. Once again, UV-Vis absorption spectroscopy
311 was used to monitor the amount of desorbed Ciprofloxacin. It is worth mentioning that the
312 adsorbent, after the pollutant removal, was washed with fresh water to eliminate the not adsorbed
313 pollutant and then swollen again in the 15 mL of salt solution for release.
314
315 **2.13 Determination of zero-point charge of Kiwi Peels.** The pH of zero-point charge (pH_{ZPC}) of
316 Kiwi Peels was evaluated using the procedure adopted by Rizzi *et al.* (Rizzi et al., 2021). Briefly,
317 30 mL of a 5.0×10^{-2} M NaCl solution were prepared by changing the pH values from 2 to 12 (pH_i).
318 HCl and NaOH were used for the purpose. Inside each solution, 35 mg of Peels were immersed and

left for 48h under continuous stirring. Then, the solution pH value of each sample was measured before (pH_i) and after (pH_F) the swelling of Kiwi Peels. A plot of "pH_i versus pH_i " and "pH_i versus pH_F" was prepared to infer the pH_{ZPC} value. In this way, two lines are obtained: a straight line from the plot of "pH_i versus pH_i " and a curve from "pH_i versus pH_F"; the intersection of these lines represents the pH_{ZPC} value.

2.14 Photodegradation of CIP. After the removal from water, the solid-state photodegradation of adsorbed CIP was obtained by using UV, H_2O_2, and their synergistic combination also in the presence of TiO_2 as photocatalyst. Particularly, Kiwi Peels immersed in fresh water (15 mL) were irradiated with a UV lamp (UV fluorescent lamp, Spectroline, Model CNF 280C/FE, λ 254 nm, light flux 0.2 mW/cm^2; USA) at different irradiation times. The CIP's desorption was accomplished to infer the amount of photodegraded material. Indeed, the amount of photodegraded CIP was obtained by knowing the total adsorbed CIP and subtracting the desorbed amount.

All the measurements reported in this paper were performed in triplicate, and error bars were reported as standard deviation.

3. RESULTS AND DISCUSSION

3.1 Physicochemical features of Kiwi Peels.

The physical and chemical features of Kiwi Peels, before and after the CIP adsorption, were investigated. For this purpose, several techniques, *i.e.*, SEM, FTIR-ATR, and TG analyses, were used in synergy, focusing on the inner and outer Kiwi Peels surfaces. More specifically, with the inner face, we referred to the surface in strict contact with the fruit pulp (preventively removed), while the outer face is related to the external surface of fruit Peels.

3.1.1 SEM and Gas Volumetric analyses. Morphological information on the Kiwi Peels samples was obtained through SEM analyses. **Figure 1** reports the SEM images of both the inner and outer surfaces of the dried Kiwi Peels before use in CIP adsorption tests. The outer surface (**Figure 1A**), with respect to the inner one (**Figure 1B**), showed more irregular areas and cavities as well as regions dominated by fiber network structures. The difference between the inner and outer sides of the Peels can be better appreciated in **Figures S1A, B**, where images at higher magnification are reported. The findings were confirmed by gas-volumetric analysis evidencing the further presence of micropores 0.4 nm wide (average value). Additionally, a high surface area of 0.50 ± 0.05 m^2/g, important feature for the adsorption of pollutants, was inferred.

3.1.2 FTIR-ATR spectroscopy measurements. As reported in the literature (Gao et al., 2021; Rahimnejad et al., 2018; Rizzi et al., 2017; Saleh Jafer and Hassan, 2019), Kiwi Peels as lignocellulosic material expose surface polar functional groups such as alcohols, aldehydes, ketones, carboxylic, phenolic, and ether groups that should affect the adsorption process interacting with CIP. **Figure 2** shows the FTIR-ATR spectrum of the adsorbent (black line). In detail, both the inner and outer surfaces were analyzed and reported in **Figures 2A** and **2B**, respectively.

Despite the important dissimilarities observed during the SEM investigation, in FTIR-ATR spectra, significative differences in signals referred to inner and outer surfaces are absent, appearing very similar to each other in terms of surface functional groups. In particular, according to other studies (Gao et al., 2021; Rahimnejad et al., 2018; Rizzi et al., 2017; Saleh Jafer and Hassan, 2019), the band at 3307 cm^{-1} indicated the O-H vibration from phenols, lignin, and polysaccharides (*i.e.*, hemicellulose and cellulose). The bands at 2840 and 2911 cm^{-1} arose mainly from asymmetric and symmetric stretching of the C-H bonds of methyl and methylene groups present in the cellulose, hemicellulose, or lignin. These bands appeared more defined when studied on the inner Kiwi Peels surface (**Figure 2A**). The slight peak detected at 1727 cm^{-1} can be ascribed to C=O groups of hemicellulose ester or carbonyl ester of lignin. The vibration mode at 1614 cm^{-1} was due to the stretching and bending vibration of the surface hydroxyls of cellulose. Furthermore, the contribution

at around 1600 cm^{-1} could be attributed to C=O stretching vibration in conjugated carbonyl of lignin. The shoulder at around 1523 cm^{-1} is usually assigned to guaiacyl and syringyl units of lignin. The bands at 1037 cm^{-1} indicated -C-O-C- bond vibration due to the presence of cellulose and hemicellulose. Weak and not well-defined signals in the region 1100 and 1500 cm^{-1}, due to CH_3, -CH_2-, C-H moieties and polyphenolic aromatic ring C=C vibration, can still be ascribed to the presence of cellulose, hemicellulose, and lignin. The bending vibration of O-H bonds, typical of celluloses, can also be accounted for. Furthermore, in this region, the contribution of C-O vibrations of carboxylate groups and the stretching of esters, ethers, or phenol groups should be considered (Gao et al., 2021; Rahimnejad et al., 2018; Rizzi et al., 2017; Saleh Jafer and Hassan, 2019). So, the prominent presence of lignin, cellulose, and hemicellulose on Kiwi Peels was demonstrated, and the finding was further confirmed by comparing the FTIR-ATR spectrum of Kiwi Peels with the results arising from olive pomace (**Figure 2A**), another lignocellulosic agricultural waste, previously investigated for the removal of emerging pollutants from water (Rizzi et al., 2017). Indeed, olive pomace was fully characterized and showed the same features as the proposed lignocellulosic adsorbent (Rizzi et al., 2017).

3.1.3 TG analyses. The presence of different components such as dietary fibers (hemicellulose, cellulose, and lignin), bioactive compounds, and other substances in Kiwi Peel samples rendered their thermal degradation a multi-stage process. This is evidenced by the TG curves and the relative derivative analysis, DTG, reported in **Figures 2C** and **2D**, respectively.

Starting from the TG analysis of Kiwi Peels before the CIP adsorption, the presence of a general weight loss of about 10-12%, which occurs up to 200°C, due to the evaporation of physically adsorbed and weakly bounded water, and due to the decomposition of less stable compounds, was observed (Rizzi et al., 2017). The first massive mass loss was noted in the range of 200-380°C, and it can be associated with the simultaneous degradation of hemicellulose, cellulose, and lignin (Rizzi et al., 2017). It follows a second and third mass loss, partially convoluted with the first one, evidenced by a different slope in the range of 380-600°C, which is likely associated, initially to the

end of the cellulose decomposition and then, to the main process of thermal decomposition of the lignin polymer structure (Rizzi et al., 2017). Indeed, lignin thermal decomposition occurs in a wide temperature range, but the process is very slow at the beginning. The residual mass at 690°C (25-29%) evidenced that the Kiwi Peels thermal decomposition was incomplete even at a very high temperature.

The related DTG curve shows better decomposition steps with the first maximum slope at a temperature of about 365°C, followed by other minor decomposition steps at higher temperatures, evidenced by the presence of shoulders (**Figure 2D**).

3.2 The adsorption process onto Kiwi Peels.

As the first step, with the aim to evidence the great performance of Kiwi Peels, the adsorption tests were performed in the presence of different EPs: Propoxur, Atenolol, Carbendazim, Furosemide, Ciprofloxacin, Paracetamol, Tetracycline, Sulfamethoxazole, Carbamazepine, Diclofenac, Ketoprofen, Naproxen, Propranolol, and Hydrochlorothiazide. The adopted amounts are reported in **Table S1**. Interestingly, Kiwi Peels were able to remove, at the same time and with great efficiencies, most of these pollutants: particularly, as highlighted in **Table S1**, the removal of Ciprofloxacin, Tetracycline, Diclofenac, Ketoprofen, Hydrochlorothiazide, and Propranolol was observed, inferring for each pollutant the Kiwi Peels maximum adsorption capacity by using **Equation 1**. It is worth noting that, even though the adsorption capacities are not high, the recyclability of Kiwi Peels, which will be discussed in the paper, should overpass this problem, resulting in a very performant adsorbent with a long lifetime.

To better characterize this latter aspect and thus the adsorbent's performance, CIP was selected as a model pollutant among all the examined EPs due to the massive employment of fluoroquinolones drugs to treat pneumonia associated with SARS-CoV-2 during the current pandemic situation.

To quickly determine the parameters affecting the pollutant removal from water, the CIP's UV-Vis absorption spectrum was monitored to infer its concentration in water before and after the contact

with Kiwi Peels. The inset of **Figure 3** shows the UV-Vis spectra evolution of a 10.0 mg/L CIP solution, pH 7.5, in the presence of 80 mg of adsorbent at room temperature (r.t.). CIP's spectrum showed three absorption maxima at λ = 270, 323, and 335 nm, respectively, attributed to $\pi \rightarrow \pi^*$ transitions involving the aromatic rings (Rizzi et al., 2021).

It is evident how the absorbance band intensities decreased at increasing the contact time and, particularly in the first 60 minutes, 60% of CIP was successfully removed. A q_{max} of 4 mg/g was obtained. After these results, preliminary in-flux measurements were carried out to evaluate the performance of the proposed adsorbent for a possible process scaling up that will be developed in the next future. A commercial syringe-like column (3.0×5.0 cm) was filled with Kiwi Peels and swelled with water. A solution of CIP (10 mg/L) was slowly flowed through the column by a piston (see the camera picture reported in **Figure S2**). The eluted solution was collected and measured by UV-Vis spectroscopy. After 15 minutes of elution, the % of CIP adsorption was calculated using **Equation 2**, resulting in about 80% removal. It is worth mentioning that important counter pressures are absent during the experiments, even if measurements were performed for a prolonged time. After these assessments, the effect of several operational parameters, such as the amount of Kiwi Peels and/or pollutant molecule, pH and temperature values, and presence of electrolytes, were investigated to infer more information about the adsorption process.

3.2.1 Effect of CIP and Kiwi Peels amounts on the adsorption process. At first, the role of active sites to adsorb CIP onto Kiwi Peels was assessed. For this purpose, different weights of dry Peels were placed in contact with a 10 mg/L CIP solution at pH 7.5 and r.t. Then, by using **Equations 1** and **2**, the adsorption % (**Figure 4A**) and the adsorption capacities (**Figure 4B**) were calculated. Increasing the Kiwi Peels amounts from 12.5 mg to 80 mg, the % of CIP removal increased. For example, by considering 60 minutes as reference contact time, it changed from 15% to 60% for the lowest and highest Kiwi Peels quantities, respectively. In agreement with previous works involving CIP and other adsorbents materials (Azizi, 2021; Peñafiel et al., 2021; Rizzi et al., 2021), the observed results highlighted the role of free sites on the adsorbent surface, more available when the

447 amount of Kiwi Peels increased due to the increased adsorbent surface. This result was further
448 elucidated by calculating the corresponding q_t values, reported in **Figure 4B**. As a whole, the
449 adsorption capacities generally decreased when the adsorbent amount increased; however, by
450 looking at the plateau region beginning, the condition in which the equilibrium was reached, it was
451 observed later when the lowest Kiwi Peels weight was used (Rizzi et al., 2021). For example, the q_t
452 values level off after 20 and 50 minutes when the highest and lowest amount of Kiwi Peels were
453 adopted, respectively. In the presence of a greater amount of adsorbent, the adsorption sites were
454 not saturated, and the q_t values appeared reduced although the removal was high. The finding
455 confirmed that free sites on the Kiwi Peels' surface favored the CIP's adsorption, being more
456 available, especially at the beginning of the process and when the Peels' amount was high. On the
457 other hand, by reducing the Kiwi Peels amount, the sites for hosting the pollutant decreased,
458 lowering the CIP removal, and the plateau region was gained later (Li et al., 2021; Ma et al., 2021).
459 Moreover, in the first time of adsorption, the observed fast CIP removal agreed with the presence of
460 abundant functional groups interacting with CIP and weaker CIP diffusion resistance (Azizi, 2021;
461 Ma et al., 2021). However, at longer contact times, the equilibrium condition achievement in the
462 plateau region and the occupation of sites, along with the decrease in the CIP's concentration
463 gradient in the solution, slowed down the diffusion and adsorption of the molecules (Rizzi et al.,
464 2021). Furthermore, when the increase of q_t values appeared slower, the presence of repulsive
465 forces between free CIP in solution and those adsorbed onto Kiwi Peels should be considered
466 (Azizi, 2021). To better characterize the process, the CIP concentration was changed by keeping
467 constant the adsorbent amount at 25 mg, as reported in **Figures 4C** and **4D**. The experimental data
468 show as the % of the pollutant removal was not affected by the CIP concentration (**Figure 4C**),
469 while the adsorption capacity increased by increasing the CIP amount (**Figure 4D**). This
470 observation confirmed the role of the CIP concentration gradient: the larger the concentration
471 gradient, the greater the driving force, which favored the pollutants transfer from the solution bulk
472 to the adsorbent (Rizzi et al., 2021). Besides, the collisions between the pollutant, if present in a

high amount, and the active free sites of the adsorbent were favored enhancing the adsorption. Indeed, a reduction of the CIP adsorption % by increasing the pollutant concentration was not observed, indicating that, as expected, the excess of CIP molecules did not worsen the CIP competition for the limited number of binding sites onto the adsorbent surface (Azizi, 2021; Ji et al., 2021; Li et al., 2021; Ma et al., 2021; Rizzi et al., 2021). In other words, the observed results suggested that both the CIP mass transfer and its adsorption onto the Kiwi Peels surface affected the kinetics of the process (Rizzi et al., 2021).

3.2.2 Kinetic analysis. The PFO (**Equation 3**) and PSO (**Equation 4**) kinetic models, respectively, were applied for interpreting previous results (Hao et al., 2021; Ji et al., 2021; Li et al., 2021; Peñafiel et al., 2021; Rizzi et al., 2021). So, by adopting the q_t values reported in **Figures 4B** and **4D**, the kinetic analysis was performed by evaluating the effects of both CIP concentration and adsorbent amount. **Figure S3** shows the obtained results. In particular, **Figures S3A** and **S3B** report the PSO and PFO models applied to adsorption experiments performed by changing the adsorbent amounts. On the other hand, **Figures S3C** and **3D** display the same models referred to experiments where the CIP amounts were changed. From the linear fitting, the corresponding kinetic parameters were calculated and reported in **Tables S1** and **S2**. Usually, to select the more suitable kinetic model for describing the experimental process, the correlation coefficients R^2, and the comparison between $q_{e,exp}$ (the experimental adsorption capacities at the equilibrium, contact time 60 minutes) and $q_{e,calc}$ (calculated adsorption capacities, obtained by applying the kinetic equations) are considered (Hao et al., 2021; Ji et al., 2021; Li et al., 2021; Peñafiel et al., 2021; Rizzi et al., 2021). **Tables S1** and **S2** show that both models' R^2 values were acceptable. However, the comparison between $q_{e,exp}$, and $q_{e,calc}$ suggests that the PFO model appeared more suitable, even if also the PSO fitted well. The same was observed by changing the amount of Kiwi Peels. These findings can be interpreted by considering previous similar works (Azizi, 2021; Hao et al., 2021; Ji et al., 2021; Li et al., 2021; Ma et al., 2021; Peñafiel et al., 2021) discussing the kinetic relevance of chemisorption and physisorption onto the Kiwi surface. In particular, collisions between the CIP molecules and

available sites at the Peels surface and the mass transfer of CIP from solution to the adsorbent could be considered important processes (Ji et al., 2021; Li et al., 2021). However, the coordination between CIP and Kiwi Peels functional groups was also significant (Hao et al., 2021; Peñafiel et al., 2021). As a whole, the analysis of the kinetic data suggested that both kinetic models could be applied for describing the CIP adsorption behavior: the CIP, at first, diffused on the Kiwi Peels surface, it adsorbed by generating a molecules layer, and subsequently, the adsorption was controlled by internal diffusion and physical/chemical interaction (Ma et al., 2021). The role of active sites and materials features became especially evident when the amount of adsorbent was high and at the end of the process during the PSO model application. On the other hand, the CIP diffusion was the rate-limiting step when the PFO model fitted the experimental data, and this scenario was observed when in excess of pollutant and at the beginning of the adsorption. Particularly, it is commonly reported that kinetics follows this model when adsorption occurs through diffusion through the interface (Azizi, 2021; Sahoo and Prelot, 2020).

The Weber-Morris model was also adopted to clarify these aspects and to highlight the intraparticle diffusion role (Peñafiel et al., 2021; Rizzi et al., 2021, 2019b). This model is represented by **Equation 5**, and it reports that if the kinetic controlling step is the intraparticle diffusion, a straight line passing through the origin should be obtained by plotting q_t values versus $t^{1/2}$. Once again, different amounts of adsorbent (**Figure S4A**) at constant CIP concentration and different CIP concentrations were considered during the analysis by fixing the amount of the adsorbent (**Figure S4B**). Starting from **Figure S4A**, it appears that the model can be applicable, restituting a single straight line passing from the origin. So, the excess of adsorbent favored the adsorption, and the internal diffusion seemed to be the slower process (Peñafiel et al., 2021; Rizzi et al., 2021). In accordance with these results, intraparticle diffusion acquires kinetic relevance when CIP concentration is reduced at a constant adsorbent amount (**Figure S4B**). Indeed, the active sites onto the adsorbent surface were more available under this condition. On the other hand, multiple segments were necessary to describe the process for higher CIP amounts, evidencing as the

adsorption involved more kinetic relevant steps, besides the intra-particle diffusion. In particular, during the first step, at the beginning of the process (described by the first straight line), the CIP diffusion, from the solution to the external adsorbent surface, played a key role (external diffusion). Afterward, there was the second step, referred to intra-particles diffusion (internal diffusion) and adsorption (usually find as the third stage in which the equilibrium was achieved) described by the second straight line at prolonged contact time (Peñafiel et al., 2021). During the second step, since the CIP concentration in solution decreased and the q_t increased, the adsorption process slowed down, hindering the CIP adsorption, and that step acquired a kinetic relevance.

3.2.3 Thermodynamic analysis. The thermodynamic parameters related to the CIP adsorption onto Kiwi Peels were determined by evaluating the temperature role. For this purpose, different temperature values were studied, from 283 to 323K, in a solution containing 25 mg of adsorbent and 10 mg/L CIP at pH 7.5. The % of CIP removal and the corresponding q_t by the temperature variation are reported in **Figures 5A** and **5B**. From 283 to 303 K, the CIP adsorption increased (see *the inset* in **Figure 5B**, in which the % of CIP adsorption at 60 minutes is reported to evidence the temperature role) at increasing the temperature values evidencing the endothermic character of the process (Hao et al., 2021; Peñafiel et al., 2021; Rizzi et al., 2021, 2019a). The temperature effect was more pronounced at the beginning of the process due to the presence of more available sites to host CIP. However, a further temperature increase lowered the CIP removal percentage (see *the inset* in **Figure 5B**), with a clear deterioration to 323K. This effect suggests the endothermic character of the adsorption process, but, at the same time, it could indicate competition between adsorption and desorption processes after a certain value of temperature. With the temperature increase, the attractive interactions between the adsorbent surface and the pollutant weaken, worsening the sorption.

So, considering the results obtained in the range of temperature 283-303K, the q_t values and the amount of the not adsorbed CIP were used to calculate the K_{eq}, at each temperature. **Equation 6** was then applied to obtain the $\Delta G°$ values reported in **Table 2**.

In general, the absolute value of the ΔG° for a physisorption process was smaller than that attributed to chemisorption. In particular, in the former case, it ranges from -20 to 0 kJ/mol, while, in the second case, it varies from -80 to -400 kJ/mol (Yu et al., 2001). So, the values of standard free energy calculated for CIP onto Kiwi Peels in the 283-305K temperature range agreed with a physisorption process, being between -20 and 0 kJ/mol. Moreover, it is also possible to say that since the $|\Delta G°|$ increments at increasing the temperature, the adsorption process was spontaneous and more favorable up to 305K.

By using **Equation 7**, by plotting $ln(K_{eq})$ versus $1/T$ (**Figure 5C**), the values of $\Delta H°_{298}$ and $\Delta S°_{298}$ were also calculated and reported in **Table 2**. The positive value of $\Delta H°_{298}$ (+40 kJ/mol) confirmed the endothermic character of the process. While, in agreement with other investigations (Peñafiel et al., 2021), the low $\Delta H°_{298}$ value corroborated the involvement of physical interactions in the CIP adsorption as confirmed by the observed effects during the rise of temperature (Ma et al., 2021; Peñafiel et al., 2021; Rizzi et al., 2021, 2019a). The $\Delta S°_{298} > 0$ (+200 J/mol×K) reflected, in turn, the affinity of CIP for Kiwi Peels and proposed the role of some structural changes in adsorbent and adsorbate in the increases the randomness at the adsorbent–adsorbate interface (Yao et al., 2010).

3.2.4 Isotherms of adsorption. The linearized forms of Langmuir, Freundlich, Temkin, and Dubinin-Radushkevitch (D-R) isotherm models (**Equations 8-13**) were applied to experimental data (Rizzi et al., 2021).

Figure 6 reports the obtained results. The R^2 values (**Table 3**), evaluated from the linear fitting, suggested, as a whole, the applicability of all the models, except for the Langmuir one. However, the best correlation was obtained when the Freundlich model was used (R^2=0.9902). **Table 3** reports the calculated isotherm parameters for each applied model. So, it can be possible to assess that the CIP adsorption was heterogeneous and the adsorbent–adsorbate interactions affected the surface coverage, inducing changes in the heat of adsorption during the process as postulated by the Freundlich model (Hao et al., 2021). This observation agreed with the heterogeneity shown by the inner and outer Kiwi Peels surfaces during the SEM analysis.

Furthermore, the value of the *n* parameter (see **Table 3**) from the Freundlich equation represents the adsorption strength, and values of 1/*n* ranging from 0 to 1, obtained during this work, confirmed that the physical CIP adsorption process was favored (Azizi, 2021; Li et al., 2021; Ma et al., 2021). Finally, when the D-R model was employed (usually used to illustrate the adsorption characteristics (Ma et al., 2021)), it fitted the experimental data with the parameters reported in **Table 3**. Although the R^2 was not very good, the q_{max} experimentally obtained (4 mg/g) agreed with the Q_0 value resulting from the fitting. An E value of 0.5 KJ/mol was calculated. So, since it was < 8 KJ/mol, it confirmed that the adsorption process involved mainly the physisorption. This hypothesis was consistent with the calculated values of $\Delta G°_{298}$ and $\Delta H°_{298}$ and is beneficial for the adsorbent regeneration due to the presence of weak interaction (Ma et al., 2021; Rizzi et al., 2021).

3.2.5 Effect of pH. The nature of the interaction between CIP and Kiwi Peels was assessed by changing the pH values of solutions containing CIP during the adsorption. CIP solutions, 10.0 mg/L, with pH values ranging from 2 to 12, were prepared and placed in contact with 25 mg of adsorbent. As reported in **Figures 7A** and **7B**, the % of adsorbed CIP and the corresponding q_t values were maxima in the range of pH 6-8 and decreased by lowering and increasing the pH values around this range (see also the *inset* in **Figure 7B**, in which the CIP % of adsorption, at 60 minutes, is reported at several pH values). If, on the one hand, when the pH was fixed at 2, the CIP adsorption was absent; on the other hand, it was slightly present at pH 9 and 12. This pH-dependent behavior has already been observed in other papers (Eze et al., 2021; Gao et al., 2021; Hao et al., 2021; Ji et al., 2021; Li et al., 2021; Ma et al., 2021; Peñafiel et al., 2021). This suggested the prominent presence of an ion-exchange mechanism involving electrostatic interactions between CIP and the main functional groups present on the adsorbent surface.

However, to better clarify this result, the pK_a values of CIP and the PZC of Kiwi Peels were considered.

As reported in **Figure 7C**, the drift method was applied to calculate the PZC of the adsorbent (Rizzi et al., 2021) that occurred positively and negatively charged at pH < 4 and >4, respectively. So, a

603 pH_{PZC} value around pH 4 was proposed. As suggested by Gao *et al.*(Gao et al., 2021), during the
604 study of lignin-based adsorbents, the large presence of carboxylic groups (as observed by the FTIR-
605 ATR analysis) could be responsible for this result. Since they are deprotonated up to pH 4, they
606 confer a net negative charge to Kiwi Peels' surface. At pH < 4, the protonation of some functional
607 groups should be expected, giving the adsorbent a positive charge.
608 Regarding CIP, the molecule presents two pKa values, $pKa_1 \approx 6$ and $pKa_2 \approx 8$, which refer to the
609 carboxylic acid group and piperazine moiety deprotonation, respectively (Azizi, 2021; Eze et al.,
610 2021; Gao et al., 2021; Hao et al., 2021; Ji et al., 2021; Li et al., 2021; Ma et al., 2021; Peñafiel et
611 al., 2021; Rizzi et al., 2021). On this basis, CIP was a cation (CIP^+) at pH < pKa_1, zwitterion ($CIP^{\pm}$)
612 in the range pK_{a1} < pH < pK_{a2}, or anion (CIP^-) at pH > pKa_2. So, the different adsorption behavior
613 could be rationalized by considering the different affinity of CIP species to Kiwi Peels that, at the
614 same time, changed their surface charge according to the adopted pH (see **Scheme 1A**) (Eze et al.,
615 2021; Gao et al., 2021; Hao et al., 2021; Ji et al., 2021; Li et al., 2021; Ma et al., 2021; Peñafiel et
616 al., 2021). At pH < 4, CIP and the adsorbent repelled each other, being both positively charged. As
617 expected, the repulsion was more evident at pH 2, where the CIP^+ was not adsorbed (Hao et al.,
618 2021). In addition, CIP is reported to be more soluble in an acid solution, making adsorption more
619 difficult (Peñafiel et al., 2021). So, CIP was still present as a cation in the pH range between 4 and
620 6, while the adsorbent was negatively charged. The contaminant removal was enhanced due to the
621 attraction between CIP^+ and the negative surface of Kiwi Peels, with an adsorption maximum at pH
622 6. As a result, the clear and main presence of electrostatic interaction between the carboxylic
623 moieties onto the adsorbent surface and CIP^+ could be evidenced. In the range of pH between the
624 two pK_a (6 < pH < 8), CIP was a zwitterion, and two different charged groups of CIP should be
625 taken into account, *i.e.*, the negative carboxylic groups and the positively charged amino moiety (Ji
626 et al., 2021). Since, in this pH range, electrostatic attraction and repulsion coexist, the CIP
627 adsorption appeared slightly decreased, likely due to the prevalence of repulsion between CIP's
628 negatively charged carboxylic group and the adsorbent (Ji et al., 2021).

At pH > 8, the CIP was present mainly as an anion, and the adsorption collapsed due to the strong repulsion between the negative charges of CIP^- and the adsorbent (Azizi, 2021; Eze et al., 2021; Gao et al., 2021; Ji et al., 2021; Li et al., 2021; Ma et al., 2021). As reported elsewhere (Gao et al., 2021; Li et al., 2021; Ma et al., 2021; Peñafiel et al., 2021), the presence of less important interactions involving H-bonds, the C=O coordination of CIP, and hydrophobic interaction between CIP and the adsorbent cannot be completely excluded contributing towards the adsorption (Gao et al., 2021; Li et al., 2021; Ma et al., 2021; Peñafiel et al., 2021).

Indeed, by looking at the results reported in **Table S1**, and thus the different nature of pollutants, the synergistic action of both electrostatic and hydrophobic interaction should be taken into account. An interesting example is the removal of Propranolol and the lack of adsorption of Atenolol observed during this work. These two molecules are very similar, differentiating for the presence of the anthracene moiety present only in the chemical structure of Propranolol. Moreover, Atenolol presents two amino functionalities that could be protonated, making the molecule according to the pH. As a result, by adopting this example, it arises that the electrostatic interaction should not work alone but work in synergy with other less intense interactions. According to Fu *et al.*(Fu et al., 2021), it is possible to assess that carboxylates groups on the Kiwi Peels surface should play a key role during the process, being involved in electrostatic interaction and hydrophobic, π-π electron donor–acceptor interactions and hydrogen bonding with CIP. The fluorine atom present on CIP could allow it to act as a π-electron acceptor, while the phenolic hydroxyl groups on Kiwi Peels surface can act as π-electron donors, favoring π–π interactions enhancing the adsorption. Furthermore, the H-bond between OH moieties onto the Kiwi surfaces and the protonated amino groups of CIP could also be considered (Fu et al., 2021).

3.2.6 Effect of salts in CIP solutions. Experiments of adsorption were performed by increasing the ionic strength of CIP solutions to confirm the presence of electrostatic interaction between Kiwi Peels and CIP (Fu et al., 2021; Gao et al., 2021; Ji et al., 2021; Rizzi et al., 2021). For this reason, in the beginning, different concentrations of NaCl were adopted to investigate CIP removal. Once

again, the q_t values and % of CIP adsorption were calculated (**Figures 8A** and **8B**). A CIP solution of 10 mg/L containing 25 mg of adsorbent at pH 7.5 was employed. In this condition, CIP was present as a zwitterion, and the adsorbent was negatively charged.

The results showed that by increasing the salt concentrations from 0.01 M to 0.3 M, the CIP's removal decreased, and the effect was more evident in the presence of NaCl 0.1 and 0.3 M, reducing the CIP removal % from 30 %, in the absence of salt, to 10 %, in the presence of NaCl, by fixing 60 minutes of contact time. This behavior was already observed in other works related to the CIP's removal (Fu et al., 2021; Gao et al., 2021; Ji et al., 2021; Rizzi et al., 2021), confirming how the adsorption process mainly involved electrostatic interactions. The observed trend was attributed to possible shielding effects of cations/anions–mediated charges both referred to as CIP functional groups and the adsorbent surface. But also competition effects involving the pollutant and ions (cations, in this case) for the adsorbent's negatively charged surface (see **Scheme 1B**) cannot be excluded (Fu et al., 2021; Gao et al., 2021; Ji et al., 2021; Rizzi et al., 2021). In particular, it should be supposed that Na^+ shielded the negative surface of the adsorbent, hindering the adsorption, and, at the same time, Na^+ can be regarded as a competitor for Kiwi Peels' surface. Besides, the salt-derived anions or cations could shield the CIP charges affecting the adsorption (**Scheme 1B**). In particular, the anions and cations could shield the protonated CIP amino moiety and the deprotonated carboxylic group, respectively.

However, to infer more information about the latter hypotheses, the effect on the adsorption process was studied by changing the nature of both anions and cations (Rizzi et al., 2021). By choosing 0.1 M as reference electrolyte concentration (when the NaCl effect was relatively strong), the salt type was changed by maintaining constant the anion (Cl^-) and changing the nature of cation: Li^+, Na^+, K^+, Mg^{2+}, and Ca^{2+}. For the sake of comparison, in **Figure 8C**, the % of CIP removal in the presence of salts was reported, selecting 60 minutes of contact time. The CIP's removal percentage decreased from K^+ to Li^+, therefore by increasing the hydrated radius of cation (K^+ = 2.32, Na^+ = 2.76 and Li^+ = 3.4 Å) (Rizzi et al., 2020b). Furthermore, by changing the cation charge from

monovalent to divalent ions, this effect appeared more pronounced by adopting Ca^{2+} and Mg^{2+} (Fu et al., 2021; Gao et al., 2021; Ji et al., 2021; Rizzi et al., 2021). Indeed, the electrical double layer on the adsorbent surface should be further compressed by increasing the solution ionic strength with divalent ions. At the same time, the coordination of cations by the negatively charged carboxylic groups cannot be excluded due to the CIP features, as already observed by Rizzi *et al.*(Rizzi et al., 2021). This effect would be expected greater for divalent cations, hindering the CIP adsorption and favoring the CIP coordination in solutions. Therefore, these observations clearly confirmed the presence of electrostatic interactions involving an ion-exchange mechanism between the CIP's functional groups and Kiwi Peels, evidencing the cations' shielding/competition effects during the adsorption (Fu et al., 2021; Gao et al., 2021; Ji et al., 2021; Rizzi et al., 2021).

Finally, the nature of anions was also changed by selecting Na^{+} as a cation, and **Figure 8D** shows the obtained results. In this case, the % of CIP removal was compared by adopting, once again, 60 minutes as contact time, but in the presence of NaCl, NaBr, NaI, and $NaClO_4$. The lack of significant differences suggested that the shielding effect of anions on CIP was not important, confirming how the cations played the main role in highlighting the probable main presence of competitive effects for the adsorbent surface.

3.2.7 Desorption of CIP and adsorbent recycling. According to the circular economy and green chemistry principles, desorption experiments were performed to assess Kiwi Peels and CIP recycling. As the first step, the role of temperature was investigated. Indeed, in **Figure 3**, it was shown that for T > 313 K, the CIP removal was reduced, stopping the adsorption at 323 K. For that reason, after the CIP's adsorption cycle, the Kiwi Peels were placed, under continuous stirring, in contact with hot water at 313 and 323K. After 60 minutes of contact time, the measured % of desorbed CIP were 60 and 75%, respectively. This observation confirmed the hypothesis that the reduced adsorption capacity of Kiwi Peels observed at T > 300K (Inset of **Figure 5B**) was attributable to the desorption effect stimulated by high temperatures. Since it is an endothermic

process, it competes with adsorption, especially by incrementing the temperature at values higher than 300K.

So, as an alternative approach to avoid hot water, the use of salts was subsequently investigated using the electrolytes that strongly affected the CIP adsorption. NaCl, $MgCl_2$, and $CaCl_2$ solutions were selected and compared by exploring different concentrations. Once again, the % of desorbed CIP was calculated (**Figures 9A**). In particular, after the CIP adsorption, as detailed during the desorption with hot water, Kiwi Peels were placed under continuous stirring in contact with the electrolytes' solutions for 60 minutes. Regarding NaCl, by increasing its concentration from 0.1 to 1 M, the % of the desorbed CIP increased from 50 % to 70 %. Instead, the CIP's release was more pronounced by using $MgCl_2$ and $CaCl_2$: in this case, the release was favored already at lower concentrations, *i.e.,* 0.1M, obtaining the 80% of contaminant's desorption without concentration effects. The findings evidenced the behavior already observed during the study about the ionic strength role, confirming the great effect of divalent cations as competitors for the Kiwi Peels surface during the ion exchange process. Therefore, a 0.1 M $MgCl_2$ solution was selected to study Kiwi Peels' ability to work under continuous adsorption/desorption cycles. **Figure 9B** reports the % of the adsorbed/desorbed CIP by adopting a contact time of 60 minutes for each cycle. Interestingly, after the second cycle, the % of adsorbed CIP increased from 27% to about 50%, and after that remained constant. The % of desorbed CIP changed from 80%, for the first desorption, to the approximately constant value of 70%, for all the subsequent runs. So, the adsorption/desorption process remained still performant, ensuring the recycling of the adsorbent/pollutant according to the green chemistry and green economy principles. However, other experiments were performed to clarify the observed behavior to get insight into the process and thus explain the improved adsorption after the 2nd cycle.

For this purpose, Kiwi Peels, before the adsorption, were placed for 60 minutes in (i) water, in (ii) a solution of 0.1M/0.5M $MgCl_2$, and for the sake of comparison also in (iii) solutions of 0.1M $CaCl_2$ and NaCl. The q_t values (**Figure S5A**) and the related % of CIP adsorption (**Figure S5B**) were

calculated. By comparing these results with those referred to dry Kiwi Peels, the treatment with $CaCl_2$ and NaCl did not affect the CIP adsorption. Conversely, a slight improvement was observed for the sample placed previously in water and used as a wet adsorbent (wet Kiwi Peels). Moreover, the use of $MgCl_2$ significantly improved both the adsorption capacities and the % of CIP's removal, and the effect seemed to be $MgCl_2$ dose-dependent indicating the important role of Mg^{2+} ions in the recycling. In agreement with these results, the % of Kiwi Peels' swelling in water was calculated by using the following relation: $\left(\frac{Weight_{wet\ Kiwi\ Peels} - Weight_{dry\ Kiwi\ Peels}}{Weight_{dry\ Kiwi\ Peels}}\right) \times 100$. In particular, the adsorbent swelling, measured at equilibrium after 5 minutes of contact time, changed from 125%, for samples previously placed in water, to 300% for the adsorbent after the contact with 0.1M $MgCl_2$ solution. On the other hand, the same 125 % swelling was also measured for the adsorbent in contact with 0.1M $CaCl_2$ and NaCl solutions. Based on these data, the important role of Mg^{2+} occurred. Indeed, Mg^{2+} ions competed with CIP's adsorption favoring its desorption, evidencing the affinity towards Kiwi Peels. Mg^{2+} ions were partially retained on the adsorbent surface due to their small sizes and their ability to coordinate the functional groups of Kiwi Peels during the ion exchange with CIP. So, the water migration from the bulk of solution towards the adsorbent was favored for an osmosis effect, as confirmed by the increased observed swelling values. Furthermore, the $MgCl_2$ treatment, as will be discussed in the following section during the TG investigation of the adsorbent after the adsorption/desorption cycles, altered the H-bonds networks. The CIP removal was thus enhanced after the salt treatment restituting the result reported in **Figure 9B**.

In conclusion, although the data shows a low q_t value (4 mg/g) compared to works in **Table 1**, they also indicate that it is possible to adopt multiple adsorption/desorption cycles to increase q_t. In other words, thanks to adsorption/desorption cycles that do not alter either the adsorbent or adsorbate properties, it is possible to increase lifetime with obvious q_t increment at least from 4 to 40 mg/g.

3.2.8 Physicochemical features of Kiwi Peels after the CIP adsorption and desorption. For this purpose, the same techniques used to characterize the adsorbent before its use were adopted to investigate the Kiwi Peels' morphologic properties after the CIP's adsorption and desorption. First of all, as it can be appreciated from SEM images in **Figures 1C-H**, the morphological features of both the outer and inner surfaces of the Kiwi Peels samples were retained after CIP adsorption and desorption, even after 10 adsorption/desorption cycles.

Interestingly, the FTIR-ATR analysis of Kiwi Peels after the CIP adsorption (**Figures 2A** and **2B**), especially when the Kiwi Peels' inner surface was considered (**Figure 2A**), evidenced slight changes. In detail, the band at 1614 cm^{-1} moved to 1621 cm^{-1} and appeared less defined, denoting the interaction of CIP with cellulose OH moieties (Fu et al., 2021; Gao et al., 2021; Rahimnejad et al., 2018; Rizzi et al., 2017; Saleh Jafer and Hassan, 2019). Accordingly, at 3307 cm-1, the OH signal decreased its relative intensity and slightly shifted, suggesting the possible formation of an H-bond with CIP (Fu et al., 2021; Rizzi et al., 2017). Moreover, the interaction between the C=O groups of lignin and CIP cannot be excluded. The bands in the region 1100-1500 cm^{-1}, ascribed to aromatic rings vibration of lignin and/or CH_3, $-CH_2-$, C-H moieties vibration of cellulose and hemicellulose, and at 1037 cm^{-1} also occurred slightly modified, changing their relative intensities. As a whole, these observations confirmed (i) the formation of H-bonds, besides the main presence of electrostatic interaction, and (ii) the possible contributions of hydrophobic forces, between CIP and Kiwi Peels, during the adsorption. Finally, after the adsorbent recycling (**Figures 2A** and **2B**), in agreement with SEM results, the lack of important changes in IR bands position, shape, and relative intensity were observed for both the Kiwi Peels surfaces. This suggested that the main adsorbent functional groups and features were not affected during the prolonged adsorption/desorption runs.

As for the TG investigation, the following results were obtained: in line with the previous discussion, the TG profiles of the Kiwi Peels sample before and after the adsorption of CIP were practically superimposable (**Figures 2C** and **2D**), as already observed with other adsorbent

materials (Rizzi et al., 2021), with a maximum rate at 360°C, corresponding to a mass loss of about 40%. The two shoulders on the DTG curve (**Figure 2D**), at 413°C and 451°C, indicated the temperatures at which the secondary decomposition processes had the maximum rate and corresponded to mass residuals of 45 and 37%, respectively.

Compared with the SEM and FTIR-ATR analyses, important thermal changes were observed when the desorption was induced with $MgCl_2$ solution. After the first cycle of adsorption/desorption using an $MgCl_2$ solution, a slight shift of the TG curve occurred at a lower temperature with a maximum decomposition rate at 355°C. After 10 adsorption/desorption cycles, this effect increased, and the maximum decomposition rate resulted at 310°C, that is a temperature lower than 50 degrees, and with a weight decrease of 30% (blue curve in **Figure 2C**) and not 40% as previously observed (red and green curves in **Figure 2C**). At higher temperatures, there was only a well-evident shoulder at 413°C, probably due to the complete overlapping of consecutive degradation steps. These results agreed with Liu's studies on the catalytic effect of $MgCl_2$ on the pyrolysis of cellulose (Liu et al., 2015): the presence of $MgCl_2$ weakened the hydrogen bonding networks, producing strong cross-linking reactions that enhanced the cellulose conversion in sugars and hence favored the decomposition. At the same time, Mg^{2+} could catalyze the re-polymerization reactions, which partially suppressed the formation of the volatile compounds justifying the lower mass reduction. So, the use of $MgCl_2$ partially affected the thermal features of Kiwi Peels and their surface, justifying the results observed when the consecutive cycles of adsorption/desorption were performed, observing the enhanced removal of CIP (**Figure 7**).

3.2.9 Removal of other pollutants and their mixtures. The Kiwi Peels' great performances were further highlighted by showing its ability to remove different emerging pollutants. By considering the results reported in **Table 1**, the removal of CIP, PRO, TC, DCF, Kp, and HTCZ was studied using solutions containing two pollutants (CIP and PRO), three pollutants (CP, PRO, and TC), and six pollutants (CIP, PRO, TC, DCF, Kp, and HTCZ). The processes were studied by adopting the UV-Vis spectroscopy as discussed before for the CIP removal. It is worth mentioning that each

808 contaminant showed its typical UV-Vis absorption spectrum that contributes to the UV-Vis
809 absorption spectrum of the mixture. As a result, an envelope of bands occurred due to the
810 superimposition of spectra ascribed to each EC. **Figures 10A**, **10B,** and 10**C** report the obtained
811 results.
812 The UV-Vis spectra were collected after 1h and 24h. As can be observed in **Figure 10**, although
813 present in complex solutions, the pollutants were successfully eliminated from the water with high
814 efficiencies of adsorption under the experimental conditions of work. These results are promising
815 and could open novel horizons in wastewater treatment because the same low-cost and
816 environmentally friendly adsorbent can adsorb many different pollutants without the important
817 effects of competition.
818 *3.2.10 Preliminary information about the CIP photodegradation after the adsorption on Kiwi Peels.*
819 As an alternative to the desorption processes, the paper focuses on the possibility of inducing the
820 solid-state photodegradation of the adsorbed CIP, offering another way for the adsorbent recycling.
821 In particular, the attention was focalized on the synergistic use of UV light, H_2O_2, UV/TiO_2, and
822 UV/H_2O_2/TiO_2.
823 As well known, •OH is one of the most important radical species produced by the adopted AOPs
824 (Rizzi et al., 2020b, 2020a, 2019a). It is highly reactive and non-selective and favors the fast
825 degradation of organic substrates. The TiO_2 and H_2O_2 co-presence together with UV-light should
826 favor the formation of additional •OH, exploiting the photocatalytic activity of TiO_2 and photolysis
827 of the peroxidic bond in H_2O_2, respectively (Rizzi et al., 2020a, 2019a). In particular, to evaluate the
828 % of photodegraded CIP, the difference between adsorbed and released CIP was calculated,
829 measuring the amount of CIP released in $MgCl_2$ (by choosing 1h as contact time with the $MgCl_2$
830 solution) after the AOPs treatment performed on CIP adsorbed onto Kiwi Peels (Rizzi et al., 2020a,
831 2019a).
832 As the first step, knowing that the CIP can be easily photodegraded in solution (Bobu et al., 2013;
833 Shah et al., 2018), the photodegradation of CIP in solid-state after its adsorption onto Kiwi Peels

was investigated. Following the previously detailed experimental procedure, the adsorbent was placed in water and irradiated with a UV lamp at different irradiation times, *i.e.*, 1, 2, and 4 h (**Figure S6**). As can be observed in **Figure S6**, the CIP photodegradation occurred, and it is influenced by the irradiation time. Indeed, by changing the irradiation time from 1 to 4h, the % of photodegraded CIP passed from 70 to 90%, indicating that the adopted approach worked well and could be suitable for the purpose. Subsequently, the use of UV-light in synergy with different concentrations of H_2O_2 was investigated by adopting 1h as the reference irradiation time. It is worth mentioning that the degradation in the presence of H_2O_2 without UV-light was not observed. Although an improved photodegradation was expected due to the UV-light and H_2O_2 joint action, the obtained results instead showed a clear reduction of the CIP photodegradation. In particular, the lowest amount of H_2O_2 (0.005M) did not affect the CIP degradation, while a slight improvement was observed by using H_2O_2 0.01M. A further increase of H_2O_2 concentration to 0.05M and 0.1M hindered the CIP degradation. The finding could be attributed to the fact that H_2O_2 was present in the solution surrounding Kiwi Peels, and the recombination of hydroxyl radicals, present in large amounts, quickly should occur according to the following processes:

$2HO\bullet \rightarrow H_2O_2$

$H_2O_2 + HO\bullet \rightarrow H_2O + HOO\bullet$

with the peroxyl radical usually less reactive than HO•. These processes retarded or completely blocked the •OH migration towards the Kiwi Peels surface, preventing the CIP degradation. The same effect was observed in the presence of TiO_2 (1 mg in 15 mL of water surrounding the adsorbent), where no improvement was detected compared to the results obtained using only UV-light with 1h as irradiation time. The results worsened if H_2O_2 0.1 M was added to the system containing TiO_2. Once again, these observations confirmed that the produced hydroxyl radicals were quickly self-quenched in solution hindering the CIP degradation. Moreover, since TiO_2 was placed in the solution, it should partially screen the UV light.

So, these preliminary results show the possibility of also adopting this alternative strategy for adsorbent regeneration. Indeed, after the CIP photodegradation, the same Kiwi Peels were recycled and used again to adsorb other CIP from a solution 10 mg/L. As already observed in **Figure 7B**, the adsorption appeared high, unveiling the concrete possibility of performing several cycles of CIP adsorption and degradation. Once again, SEM, FTIR-ATR, and TG analyses were used in synergy to characterize the adsorbent after the CIP solid-state photodegradation. For the sake of comparison, only some of the explored conditions described in **Figure S6** are reported: after UV-irradiation for 4h, UV irradiation using H_2O_2 0.01 M and 0.05 M, UV irradiation using H_2O_2 (0.01M) and TiO_2 and after UV irradiation in the presence of TiO_2. SEM analysis carried out on both the outer and inner surfaces of the Kiwi Peels samples confirmed the lack of significant morphological changes also after use in AOPs (**Figures S7** and **S8).** In agreement with the SEM investigation, the FTIR-ATR analysis showed that the outer Kiwi Peels surface, after the treatments with UV-light, H_2O_2, and TiO_2, appeared unaffected (*data not shown*), exhibiting the same spectrum reported in **Figure 2B**. Instead, the inner Peels surfaces resulted slightly modified according to the FTIR-ATR spectrum reported in **Figure S9**. Though the spectra were very similar to those recorded for Kiwi Peels before the treatments, some slight changes were noted, especially in the 1400-1800 cm^{-1} wavenumber region. In particular, the ratio between the band at 1640 cm^{-1} and that at 1523 cm^{-1} changed in favor of the latter (indicated with an asterisk in **Figure S9**), suggesting the slight and partial lignocellulosic material oxidation, confirmed by the TGA and DTG of some samples reported in **Figures S10** and **S11**. The UV irradiation gives rise to structural modifications that make the adsorbent less stable with maximum decomposition rate temperatures between 325 and 340°C and comparable mass loss, and the most pronounced effect was obtained in the presence of TiO_2.

Finally, the possibility of adsorbing the by-products of CIP photodegradation was investigated. For this purpose and as an example, a CIP solution was irradiated for 90 minutes with UV-light, and the UV-Vis spectra of this solution were collected over time (**Figure S11A**). The time evolution of the

absorption spectrum clearly evidenced the photodegradation of CIP suggested by the CIP absorbance intensity decreasing, with the presence of two isosbestic points at 306 and 345 nm, indicating a chemical reaction in progress. Interestingly, the UV light was turned off at the end of the experiments, and Kiwi Peels were swollen inside the irradiated solution. UV-Vis spectroscopy was used, once again, to monitor the adsorption process over time (**Figure S11B**). The absorbance intensity of the spectroscopic signals, attributed to CIP and its photoinduced by-products, decreased. This observation successfully evidenced the ability of Kiwi Peels to even adsorb the CIP by-products, proving to be a very effective adsorbent.

CONCLUSIONS

This work aimed to valorize the Kiwi Peels, an agricultural waste, presenting and proposing them as adsorbent material for removing emerging pollutants from water, in accordance with Circular Economy principles.

Before performing adsorption experiments, the proposed material was carefully characterized before and after the adsorption process, thanks to the synergistic use of several techniques, namely FTIR-ATR, TG, and SEM, that allowed to acquire information about the inner and outer Kiwi Peels surfaces featured by a lignocellulosic nature.

By adopting Ciprofloxacin as a model drug, the adsorption process was fully characterized. Particularly, the isotherm and the kinetic models were investigated, and, as a result, it was observed that the process was defined by the Freundlich equation. Both the pseudo-first and pseudo-second-order kinetic models well described the Ciprofloxacin removal with the applicability of the Weber-Morris equation. For recycling both the pollutant (the Ciprofloxacin) and the adsorbent material (the Kiwi Peels), since the presence of salt slowed down the process, the pollutant desorption was investigated after selecting 0.1M $MgCl_2$, and 10 cycles of adsorption/desorption were successfully performed, evidencing an increase in the adsorbent lifetime, without any drop in performances and morphological features or microstructure. Alternatively, the solid-state photodegradation of the

pollutant after the adsorption onto Kiwi Peels was further proposed and explored by using the Advanced Oxidation Processes for giving the possibility of recycling the adsorbent that. The results appeared interesting; unfortunately, the adsorbent material was partially affected by the oxidation processes; thus, the desorption of Ciprofloxacin should be preferred, and its photodegradation should be performed subsequently in solution. The possibility of using Kiwi Peels as adsorbents for the UV-light photoinduced by-products was also explored and demonstrated. In conclusion, it can be stated the valorization of a waste, the Kiwi Peels, transforming them into a resource for water remediation applications. Work is in progress to avoid the disposal of washing water derived from the pretreatment step of the Kiwi Peels into the environment to further valorize this kind of waste, thus obtaining value-added by-products.

So, the use of Kiwi Peels has the great potential to favor a new virtuous alliance between agriculture, enterprise, and research. So, the academic research will close the bioeconomic circle, giving rise to promising collaborations that will multiply the value of Kiwi fruits while improving the engineering of production processes with the development of new plant technologies to transform Kiwi wastes into value-added materials. In turn, this innovation will enhance the competitiveness of food producers and revitalize the territory.

ACKNOWLEDGEMENTS.

We gratefully acknowledge Mr. Sergio Nuzzo for his skillful and excellent technical assistance. This work was supported by “Research for Innovation (REFIN) per l’individuazione dei progetti di ricerca” - POR PUGLIA FESR-FSE 2014/2020 and by the LIFE + European Project named LIFE CLEAN UP (“Validation of adsorbent materials and advanced oxidation techniques to remove emerging pollutants in treated wastewater”) [LIFE 16 ENV/ES/000169].

Author contribution. Vito Rizzi: Conceptualization, validation, methodology, writing—review, and editing; Jennifer Gubitosa: Conceptualization, validation, investigation, writing—original draft

preparation; Domenico Cignolo: Investigation, Data Curation; Paola Fini: validation; Fiorenza Fanelli: SEM experiments; Pinalysa Cosma: formal analysis, resources, project administration, writing—review and editing, funding acquisition.

Data availability. All data analyzed during this study are included in this published article.

DECLARATIONS

Competing interests. The authors declare no competing interests.

REFERENCES

Afolabi, I.C., Popoola, S.I., Bello, O.S., 2020. Modeling pseudo-second-order kinetics of orange peel-paracetamol adsorption process using artificial neural network. Chemom. Intell. Lab. Syst. 203, 104053. https://doi.org/10.1016/j.chemolab.2020.104053

Afzal, M.Z., Sun, X.-F., Liu, J., Song, C., Wang, S.-G., Javed, A., 2018. Enhancement of ciprofloxacin sorption on chitosan/biochar hydrogel beads. Sci. Total Environ. 639, 560–569. https://doi.org/https://doi.org/10.1016/j.scitotenv.2018.05.129

Al-Qahtani, K.M., 2016. Water purification using different waste fruit cortexes for the removal of heavy metals. J. Taibah Univ. Sci. 10, 700–708. https://doi.org/10.1016/j.jtusci.2015.09.001

Aman, T., Kazi, A.A., Sabri, M.U., Bano, Q., 2008. Potato peels as solid waste for the removal of heavy metal copper(II) from waste water/industrial effluent. Colloids Surfaces B Biointerfaces 63, 116–121. https://doi.org/https://doi.org/10.1016/j.colsurfb.2007.11.013

Ashiq, A., Sarkar, B., Adassooriya, N., Walpita, J., Rajapaksha, A.U., Ok, Y.S., Vithanage, M., 2019. Sorption process of municipal solid waste biochar-montmorillonite composite for ciprofloxacin removal in aqueous media. Chemosphere 236, 124384. https://doi.org/https://doi.org/10.1016/j.chemosphere.2019.124384

959 Azizi, A., 2021. Green synthesis of iron oxide/cellulose magnetic recyclable nanocomposite and its
960 evaluation in ciprofloxacin removal from aqueous solutions. J. Iran. Chem. Soc. 18, 331–341.
961 https://doi.org/10.1007/s13738-020-02028-4

962 Balarak, D., Baniasadi, M., Lee, S.M., Shim, M.J., 2021a. Ciprofloxacin adsorption onto azolla
963 filiculoides activated carbon from aqueous solutions. Desalin. Water Treat. 218, 444–453.
964 https://doi.org/10.5004/dwt.2021.26986

965 Balarak, D., Mahv, A.H., Shimc, M.J., Lee, S.-M., 2021b. Adsorption of ciprofloxacin from
966 aqueous solution onto synthesized NiO: isotherm, kinetic and thermodynamic studies. Desalin.
967 Water Treat. 212, 390–400. https://doi.org/10.5004/dwt.2021.26603

968 Bhatnagar, A., Sillanpää, M., Witek-Krowiak, A., 2015. Agricultural waste peels as versatile
969 biomass for water purification – A review. Chem. Eng. J. 270, 244–271.
970 https://doi.org/https://doi.org/10.1016/j.cej.2015.01.135

971 Bobu, M., Yediler, A., Siminiceanu, I., Zhang, F., Schulte-Hostede, S., 2013. Comparison of
972 different advanced oxidation processes for the degradation of two fluoroquinolone antibiotics
973 in aqueous solutions. J. Environ. Sci. Heal. Part A 48, 251–262.
974 https://doi.org/10.1080/10934529.2013.726805

975 Chamorro, F., Carpena, M., Fraga-Corral, M., Echave, J., Riaz Rajoka, M.S., Barba, F.J., Cao, H.,
976 Xiao, J., Prieto, M.A., Simal-Gandara, J., 2022. Valorization of kiwi agricultural waste and
977 industry by-products by recovering bioactive compounds and applications as food additives: A
978 circular economy model. Food Chem. 370, 131315.
979 https://doi.org/10.1016/j.foodchem.2021.131315

980 Eze, S.I., Akpomie, K.G., Ezekoye, O.M., Chukwujindu, C.N., Ojo, F.K., Ani, J.U., Ujam, O.T.,
981 2021. Antibiotic Adsorption by Acid Enhanced Dialium guineense Seed Waste. Arab. J. Sci.
982 Eng. 46, 309–324. https://doi.org/10.1007/s13369-020-04771-5

983 Fan, H., Ma, Y., Wan, J., Wang, Y., Li, Z., Chen, Y., 2020. Adsorption properties and mechanisms
984 of novel biomaterials from banyan aerial roots via simple modification for ciprofloxacin
985 removal. Sci. Total Environ. 708, 134630.
986 https://doi.org/https://doi.org/10.1016/j.scitotenv.2019.134630

987 Fu, Y., Yang, Z., Xia, Y., Xing, Y., Gui, X., 2021. Adsorption of ciprofloxacin pollutants in
988 aqueous solution using modified waste grapefruit peel. Energy Sources, Part A Recover. Util.
989 Environ. Eff. 43, 225–234. https://doi.org/10.1080/15567036.2019.1624877

990 Gao, B., Chang, Q., Yang, H., 2021. Selective adsorption of ofloxacin and ciprofloxacin from a
991 binary system using lignin-based adsorbents: Quantitative analysis, adsorption mechanisms,
992 and structure-activity relationship. Sci. Total Environ. 765, 144427.
993 https://doi.org/https://doi.org/10.1016/j.scitotenv.2020.144427

994 Gothwal, R., Shashidhar, T., 2015. Antibiotic Pollution in the Environment: A Review. CLEAN –
995 Soil, Air, Water 43, 479–489. https://doi.org/https://doi.org/10.1002/clen.201300989

996 Hao, B., Wang, F., Huang, H., Wu, Y., Jia, S., Liao, Y., Mao, H., 2021. Tannin foam immobilized
997 with ferric ions for efficient removal of ciprofloxacin at low concentrations. J. Hazard. Mater.
998 414, 125567. https://doi.org/https://doi.org/10.1016/j.jhazmat.2021.125567

999 Iwuozor, K.O., Emenike, E.C., Aniagor, C.O., Iwuchukwu, F.U., Ibitogbe, E.M., Okikiola, T.B.,
1000 Omuku, P.E., Adeniyi, A.G., 2022. Removal of pollutants from aqueous media using cow
1001 dung-based adsorbents. Curr. Res. Green Sustain. Chem.
1002 https://doi.org/10.1016/j.crgsc.2022.100300

1003 Ji, H., Wang, T., Huang, T., Lai, B., Liu, W., 2021. Adsorptive removal of ciprofloxacin with
1004 different dissociated species onto titanate nanotubes. J. Clean. Prod. 278, 123924.
1005 https://doi.org/https://doi.org/10.1016/j.jclepro.2020.123924

1006 Khan, N.A., Najam, T., Shah, S.S.A., Hussain, E., Ali, H., Hussain, S., Shaheen, A., Ahmad, K.,

1007 Ashfaq, M., 2020. Development of Mn-PBA on GO sheets for adsorptive removal of
1008 ciprofloxacin from water: Kinetics, isothermal, thermodynamic and mechanistic studies.
1009 Mater. Chem. Phys. 245, 122737.
1010 https://doi.org/https://doi.org/10.1016/j.matchemphys.2020.122737

1011 Li, J., Pan, L., Yu, G., Li, C., Xie, S., Wang, Y., 2021. Synthesis of an easily recyclable and safe
1012 adsorbent from sludge pyrochar for ciprofloxacin adsorption. Environ. Res. 192, 110258.
1013 https://doi.org/https://doi.org/10.1016/j.envres.2020.110258

1014 Li, S., Zhang, X., Huang, Y., 2017. Zeolitic imidazolate framework-8 derived nanoporous carbon as
1015 an effective and recyclable adsorbent for removal of ciprofloxacin antibiotics from water. J.
1016 Hazard. Mater. 321, 711–719. https://doi.org/https://doi.org/10.1016/j.jhazmat.2016.09.065

1017 Liakos, E. V, Rekos, K., Giannakoudakis, D.A., Mitropoulos, A.C., Fu, J., Kyzas, G.Z., 2021.
1018 Activated Porous Carbon Derived from Tea and Plane Tree Leaves Biomass for the Removal
1019 of Pharmaceutical Compounds from Wastewaters. Antibiot. .
1020 https://doi.org/10.3390/antibiotics10010065

1021 Liu, D., Yu, Y., Long, Y., Wu, H., 2015. Effect of MgCl2 loading on the evolution of reaction
1022 intermediates during cellulose fast pyrolysis at 325°C. Proc. Combust. Inst. 35, 2381–2388.
1023 https://doi.org/https://doi.org/10.1016/j.proci.2014.05.026

1024 Lu, D., Xu, S., Qiu, W., Sun, Y., Liu, X., Yang, J., Ma, J., 2020. Adsorption and desorption
1025 behaviors of antibiotic ciprofloxacin on functionalized spherical MCM-41 for water treatment.
1026 J. Clean. Prod. 264, 121644. https://doi.org/https://doi.org/10.1016/j.jclepro.2020.121644

1027 Ma, J., Yang, M., Yu, F., Zheng, J., 2015. Water-enhanced Removal of Ciprofloxacin from Water
1028 by Porous Graphene Hydrogel. Sci. Rep. 5, 13578. https://doi.org/10.1038/srep13578

1029 Ma, Y., Li, M., Li, P., Yang, L., Wu, L., Gao, F., Qi, X., Zhang, Z., 2021. Hydrothermal synthesis
1030 of magnetic sludge biochar for tetracycline and ciprofloxacin adsorptive removal. Bioresour.

1031 Technol. 319, 124199. https://doi.org/https://doi.org/10.1016/j.biortech.2020.124199

1032 Mohammadi Nodeh, M.K., Soltani, S., Shahabuddin, S., Rashidi Nodeh, H., Sereshti, H., 2018.
1033 Equilibrium, Kinetic and Thermodynamic Study of Magnetic Polyaniline/Graphene Oxide
1034 Based Nanocomposites for Ciprofloxacin Removal from Water. J. Inorg. Organomet. Polym.
1035 Mater. 28, 1226–1234. https://doi.org/10.1007/s10904-018-0782-2

1036 Mokif, L.A., Abdulhusain, N.A., AL-Mamoori, S.O.H., 2018. The Possibility of Using the kiwi
1037 Peels as an Adsorbent for Removing Nitrate from Water. J. Univ. Babylon, Eng. Sci. 26, 192–
1038 197.

1039 Nassar, M.Y., Ahmed, I.S., Raya, M.A., 2019. A facile and tunable approach for synthesis of pure
1040 silica nanostructures from rice husk for the removal of ciprofloxacin drug from polluted
1041 aqueous solutions. J. Mol. Liq. 282, 251–263.
1042 https://doi.org/https://doi.org/10.1016/j.molliq.2019.03.017

1043 Obinna, I.B., Ebere, *Enyoh, 2019. A review: Water pollution by heavy metal and organic
1044 pollutants: Brief review of sources, effects and progress on remediation with aquatic plants.
1045 Anal. Methods Environ. Chem. J. 2. https://doi.org/10.24200/amecj.v2.i03.66

1046 Peñafiel, M.E., Matesanz, J.M., Vanegas, E., Bermejo, D., Mosteo, R., Ormad, M.P., 2021.
1047 Comparative adsorption of ciprofloxacin on sugarcane bagasse from Ecuador and on
1048 commercial powdered activated carbon. Sci. Total Environ. 750, 141498.
1049 https://doi.org/https://doi.org/10.1016/j.scitotenv.2020.141498

1050 Rahimnejad, M., Pirzadeh, K., Mahdavi, I., Peyghambarzadeh, S.M., 2018. Pb(II) removal from
1051 aqueous solution by adsorption on activated carbon from kiwi peel. Environ. Eng. Manag. J.
1052 17, 1293–1300.

1053 Rashed, M.N.R.E.-M.N., 2013. Adsorption Technique for the Removal of Organic Pollutants from
1054 Water and Wastewater. IntechOpen, Rijeka, p. Ch. 7. https://doi.org/10.5772/54048

1055 Rigoletto, M., Calza, P., Gaggero, E., Laurenti, E., 2022. Hybrid materials for the removal of
1056 emerging pollutants in water: classification, synthesis, and properties. Chem. Eng. J. Adv. 10,
1057 100252. https://doi.org/10.1016/j.ceja.2022.100252

1058 Rizzi, V., D'Agostino, F., Fini, P., Semeraro, P., Cosma, P., 2017. An interesting environmental
1059 friendly cleanup: The excellent potential of olive pomace for disperse blue
1060 adsorption/desorption from wastewater. Dye. Pigment. 140, 480–490.
1061 https://doi.org/10.1016/j.dyepig.2017.01.069

1062 Rizzi, V., Fiorini, F., Lamanna, G., Gubitosa, J., Prasetyanto, E.A., Fini, P., Fanelli, F., Nacci, A.,
1063 Cola, L. De, Cosma, P., 2018. Polyamidoamine-Based Hydrogel for Removal of Blue and Red
1064 Dyes from Wastewater. Adv. Sustain. Syst. https://doi.org/10.1002/adsu.201700146

1065 Rizzi, V., Gubitosa, J., Fini, P., Petrella, A., Romita, R., Agostiano, A., Cosma, P., 2020a. A
1066 "classic" material for capture and detoxification of emergent contaminants for water
1067 purification: The case of tetracycline. Environ. Technol. Innov. 19, 100812.
1068 https://doi.org/https://doi.org/10.1016/j.eti.2020.100812

1069 Rizzi, V., Gubitosa, J., Fini, P., Romita, R., Agostiano, A., Nuzzo, S., Cosma, P., 2020b.
1070 Commercial bentonite clay as low-cost and recyclable "natural" adsorbent for the
1071 Carbendazim removal/recover from water: Overview on the adsorption process and
1072 preliminary photodegradation considerations. Colloids Surfaces A Physicochem. Eng. Asp.
1073 https://doi.org/10.1016/j.colsurfa.2020.125060

1074 Rizzi, V., Gubitosa, J., Signorile, R., Fini, P., Cecone, C., Matencio, A., Trotta, F., Cosma, P., 2021.
1075 Cyclodextrin nanosponges as adsorbent material to remove hazardous pollutants from water:
1076 The case of ciprofloxacin. Chem. Eng. J. 411, 128514.
1077 https://doi.org/https://doi.org/10.1016/j.cej.2021.128514

1078 Rizzi, V., Lacalamita, D., Gubitosa, J., Fini, P., Petrella, A., Romita, R., Agostiano, A., Gabaldón,

J.A.J.A., Fortea Gorbe, M.I.M.I., Gómez-Morte, T., Cosma, P., 2019a. Removal of tetracycline from polluted water by chitosan-olive pomace adsorbing films. Sci. Total Environ. 693, 133620. https://doi.org/https://doi.org/10.1016/j.scitotenv.2019.133620

Rizzi, V., Romanazzi, F., Gubitosa, J., Fini, P., Romita, R., Agostiano, A., Petrella, A., Cosma, P., 2019b. Chitosan Film as Eco-Friendly and Recyclable Bio-Adsorbent to Remove/Recover Diclofenac, Ketoprofen, and their Mixture from Wastewater. Biomolecules 9, 571. https://doi.org/10.3390/biom9100571

Sahoo, T.R., Prelot, B., 2020. Adsorption processes for the removal of contaminants from wastewater: The perspective role of nanomaterials and nanotechnology, in: Nanomaterials for the Detection and Removal of Wastewater Pollutants. Elsevier, pp. 161–222. https://doi.org/10.1016/B978-0-12-818489-9.00007-4

Saleh Jafer, A., Hassan, A.A., 2019. Removal of oil content in oilfield produced water using chemically modified kiwi peels as efficient low-cost adsorbent. J. Phys. Conf. Ser. 1294, 72013. https://doi.org/10.1088/1742-6596/1294/7/072013

Sanz, V., López-Hortas, L., Torres, M.D., Domínguez, H., 2021. Trends in kiwifruit and byproducts valorization. Trends Food Sci. Technol. https://doi.org/10.1016/j.tifs.2020.11.010

Shah, N.S., Rizwan, A.D., Khan, J.A., Sayed, M., Khan, Z.U.H., Murtaza, B., Iqbal, J., Din, S.U., Imran, M., Nadeem, M., Al-Muhtaseb, A.H., Muhammad, N., Khan, H.M., Ghauri, M., Zaman, G., 2018. Toxicities, kinetics and degradation pathways investigation of ciprofloxacin degradation using iron-mediated H2O2 based advanced oxidation processes. Process Saf. Environ. Prot. 117, 473–482. https://doi.org/https://doi.org/10.1016/j.psep.2018.05.020

Shuaibing, Z.M.Z.S.L., Qihua, Z., 2013. Adsorption of dye wastewater by banana peel powder immobilized by sodium alginate. Chinese J. Environ. Eng. 7, 2208–2212.

Tran, T. Van, Nguyen, D.T.C., Le, H.T.N., Tu, T.T.K., Le, N.D., Lim, K.T., Bach, L.G., Nguyen,

T.D., 2019. MIL-53 (Fe)-directed synthesis of hierarchically mesoporous carbon and its utilization for ciprofloxacin antibiotic remediation. J. Environ. Chem. Eng. 7, 102881. https://doi.org/https://doi.org/10.1016/j.jece.2019.102881

Ulyankina, A., Molodtsova, T., Gorshenkov, M., Leontyev, I., Zhigunov, D., Konstantinova, E., Lastovina, T., Tolasz, J., Henych, J., Licciardello, N., Cuniberti, G., Smirnova, N., 2021. Photocatalytic degradation of ciprofloxacin in water at nano-ZnO prepared by pulse alternating current electrochemical synthesis. J. Water Process Eng. 40, 101809. https://doi.org/https://doi.org/10.1016/j.jwpe.2020.101809

Wang, L., Yang, C., Lu, A., Liu, S., Pei, Y., Luo, X., 2020. An easy and unique design strategy for insoluble humic acid/cellulose nanocomposite beads with highly enhanced adsorption performance of low concentration ciprofloxacin in water. Bioresour. Technol. 302, 122812. https://doi.org/https://doi.org/10.1016/j.biortech.2020.122812

Xu, G.F., Jing, H.M., Guo, R.X., 2014. The Adsorption Isotherm Studies of Orange Peel on Pesticide Furadan. Appl. Mech. Mater. 477–478, 1331–1335. https://doi.org/10.4028/www.scientific.net/AMM.477-478.1331

Yao, Y., Xu, F., Chen, M., Xu, Z., Zhu, Z., 2010. Adsorption behavior of methylene blue on carbon nanotubes. Bioresour. Technol. 101, 3040–3046. https://doi.org/https://doi.org/10.1016/j.biortech.2009.12.042

Yu, F., Chen, D., Ma, J., 2018. Adsorptive removal of ciprofloxacin by ethylene diaminetetraacetic acid/β-cyclodextrin composite from aqueous solution. New J. Chem. 42, 2216–2223. https://doi.org/10.1039/C7NJ03770H

Yu, Y., Zhuang, Y.-Y., Wang, Z.-H., 2001. Adsorption of Water-Soluble Dye onto Functionalized Resin. J. Colloid Interface Sci. 242, 288–293. https://doi.org/https://doi.org/10.1006/jcis.2001.7780

Zhang, H., Khanal, S.K., Jia, Y., Song, S., Lu, H., 2019. Fundamental insights into ciprofloxacin adsorption by sulfate-reducing bacteria sludge: Mechanisms and thermodynamics. Chem. Eng. J. 378, 122103. https://doi.org/https://doi.org/10.1016/j.cej.2019.122103

Zhao, F., Repo, E., Yin, D., Chen, L., Kalliola, S., Tang, J., Iakovleva, E., Tam, K.C., Sillanpää, M., 2017. One-pot synthesis of trifunctional chitosan-EDTA-β-cyclodextrin polymer for simultaneous removal of metals and organic micropollutants. Sci. Rep. 7, 15811. https://doi.org/10.1038/s41598-017-16222-7

Zheng, C., Zheng, H., Hu, C., Wang, Yili, Wang, Yongjuan, Zhao, C., Ding, W., Sun, Q., 2020. Structural design of magnetic biosorbents for the removal of ciprofloxacin from water. Bioresour. Technol. 296, 122288. https://doi.org/https://doi.org/10.1016/j.biortech.2019.122288

FIGURE CAPTIONS

Figure 1: Representative SEM images of Kiwi Peels before CIP adsorption (**A**, **B**), after CIP adsorption (**C**, **D**), after CIP desorption in 0.1 M $MgCl_2$ solution (**E**, **F**), after 10 cycles of CIP adsorption/desorption (**G**, **H**). Images of both the outer (**A**, **C**, **E**, **G**) and inner (**B**, **D**, **F**, **H**) side of the peel samples are reported.

Figure 2: Comparison between FTIR-ATR spectra (wavenumbers range 500-4000 cm^{-1}) referred to the inner (**A**) or outer Kiwi Peels surface (**B**), and TG (**C**) with the related DTG (**D**) analyses obtained for the adsorbent before and after the CIP adsorption/desorption. The Olive pomace FTIR-ATR spectrum is also reported.

Figure 3: The pollutant's chemical structure and the adsorbent's camera pictures are reported detailing the process to obtain dry Kiwi Peels. *Inset*: UV-Vis spectra of a CIP solution, 10 mg/L, pH 7.5 at r.t., in the presence of 80 mg of Kiwi Peels, collected at several contact times.

Figure 4: % of CIP adsorption onto Kiwi Peels, with the related adsorption capacities, by adopting a CIP solution 10 mg/L, at pH 7.5 and r.t., and different adsorbent amounts (**A, B**) and by changing the CIP concentrations, 2.5-20 mg/L by using 25 mg of Kiwi Peels (**C, D**).

Figure 5: Adsorption capacities (**A**) onto Kiwi Peels (25 mg) with the related % of CIP adsorption (**B**) at several temperature values (from a CIP solution 10 mg/L, pH 7.5), the *inset* reports the % of adsorption, calculated at 60 minutes, and several temperature values; Plot of $\ln(k_{eq})$ *vs.* 1/T to obtain $\Delta H°$ and $\Delta S°$ at 298 K (**C**).

Figure 6: Isotherms of adsorption: Langmuir (**A**), Freundlich (**B**), Temkin (**C**) and D-R (**D**).

Figure 7: Kiwi Peels adsorption capacities (**A**) with the related % of CIP adsorption (**B**) calculated at several pH values (from a CIP solution 10.0 mg/L in the presence of 25 mg of adsorbent); the *inset* reports the % of CIP adsorption calculated at 60 minutes and at several pH values; application of the drift method to calculate the adsorbent PZC (**C**).

Figure 8: Kiwi Peels adsorption capacities (**A**) with the related % of CIP adsorption (**B**) obtained in the presence of different NaCl concentrations; % of CIP adsorption, calculated at 60 minutes as contact time, onto Kiwi Peels by changing the cation (**C**) and anion nature (**D**) (salt concentration: 0.1 M). All the experiments are related to a CIP solution 10 mg/L, pH 7.5, in the presence of 25 mg of Peels.

Figure 9: % of CIP desorption from Kiwi Peels (calculated at 60 minutes as contact time of desorption), in the presence of different concentrations of NaCl, $MgCl_2$, and $CaCl_2$. The related adsorption was obtained from a solution 10 mg/L by adopting 60 minutes as adsorption contact time and 25 mg of Peels (**A**); Consecutive cycles of CIP adsorption, from a solution 10 mg/L (the contact time is 60 minutes, by adopting 25 mg of adsorbent) and desorption in 0.1M $MgCl_2$ (the % of desorption is calculated at 60 minutes adopted as contact time) (**B**).

Figure 10: UV-Vis spectra of a mixture of CIP and PRO (**A**), CIP, PRO and TC (**B**), CIP, PRO, TC, DCF, Kp, and HTCZ (**C**); each pollutant has a concentration of 5 mg/L, and the adsorption process is investigated in the presence of 25 mg of Kiwi Peels.

Scheme 1: A schematic illustration depicting the interaction between Kiwi Peels and CIP at several pH values (**A**) and in the presence of anions/cations from salts (**B**).

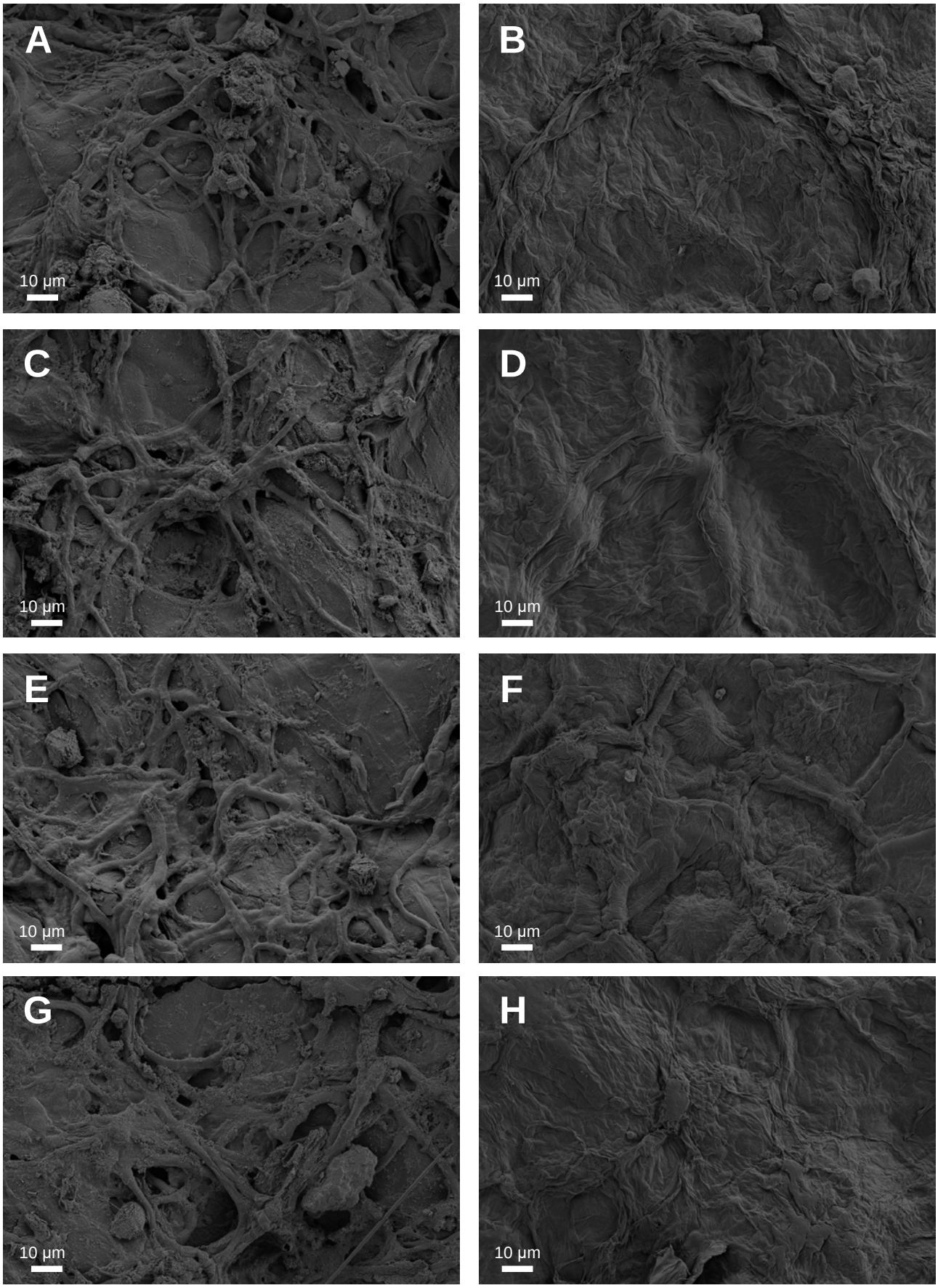

1182

1183 **Figure 1**

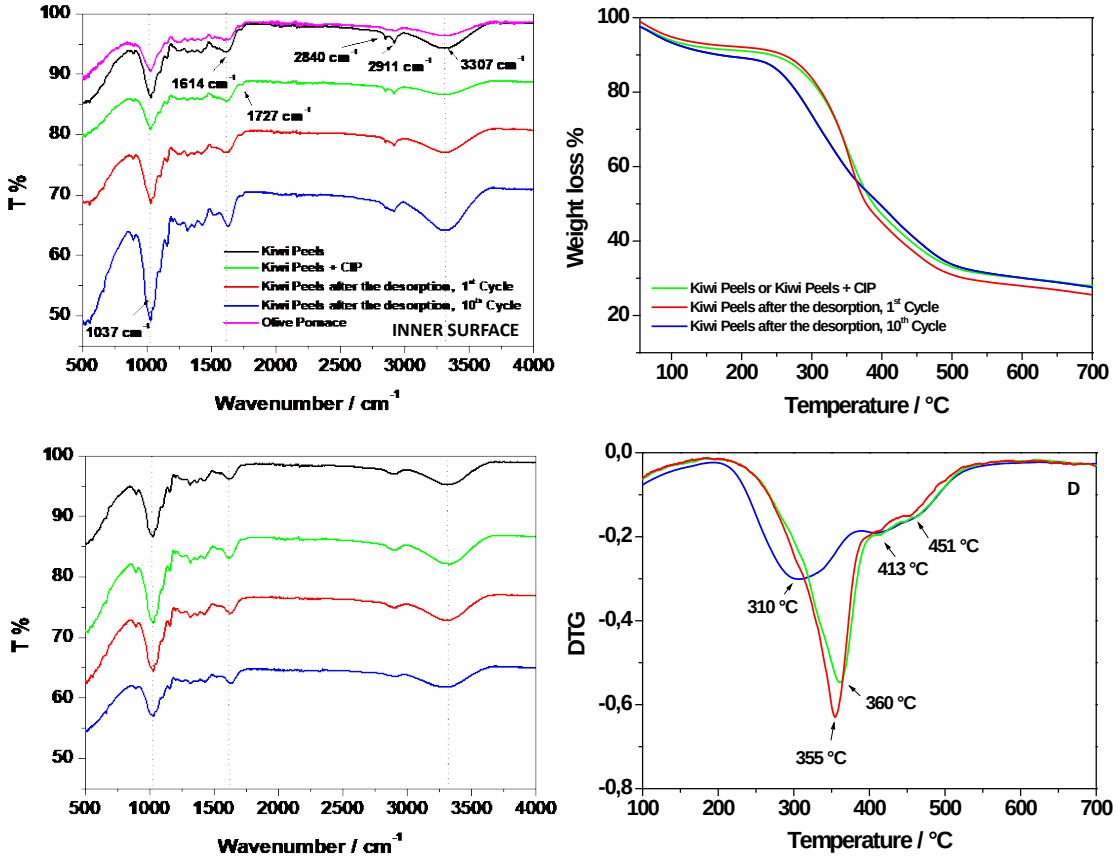

1184

1185 **Figure 2**

1186

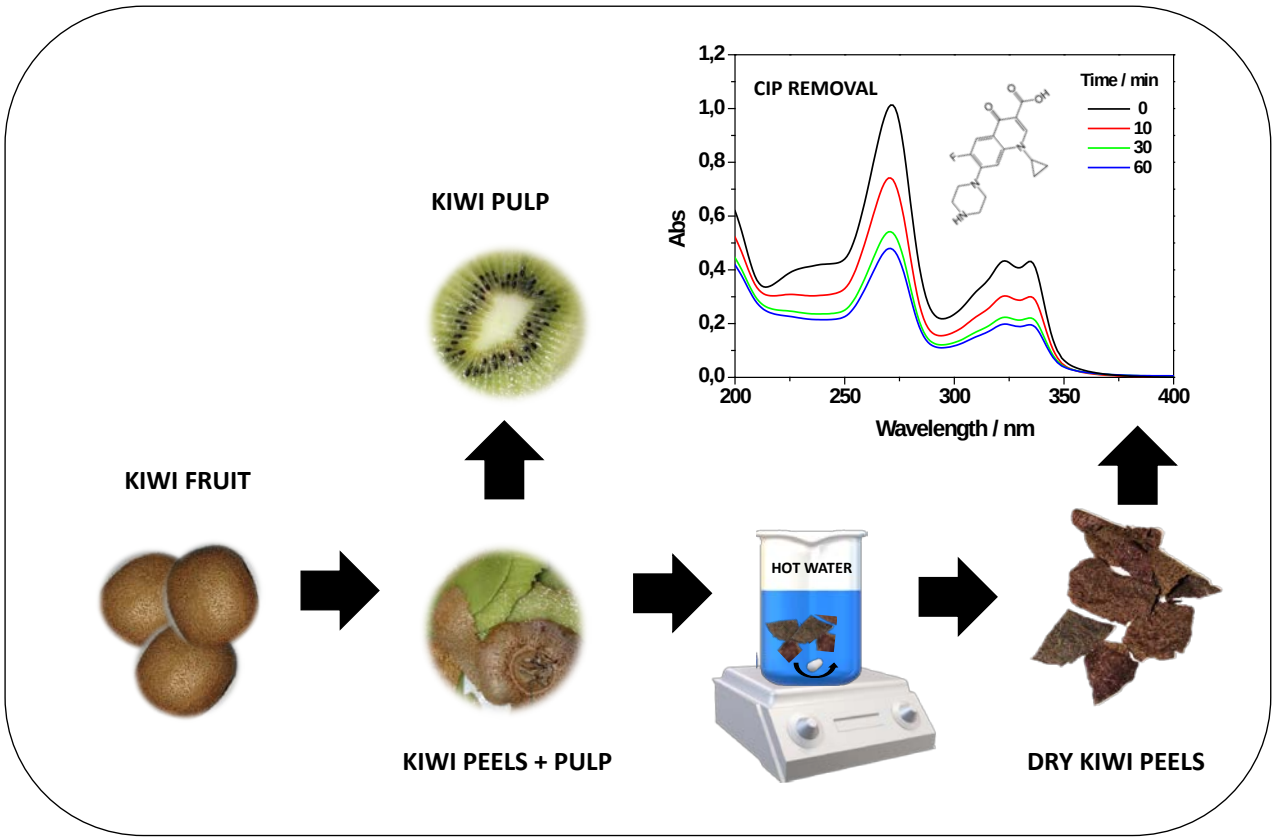

1187

1188 **Figure 3**

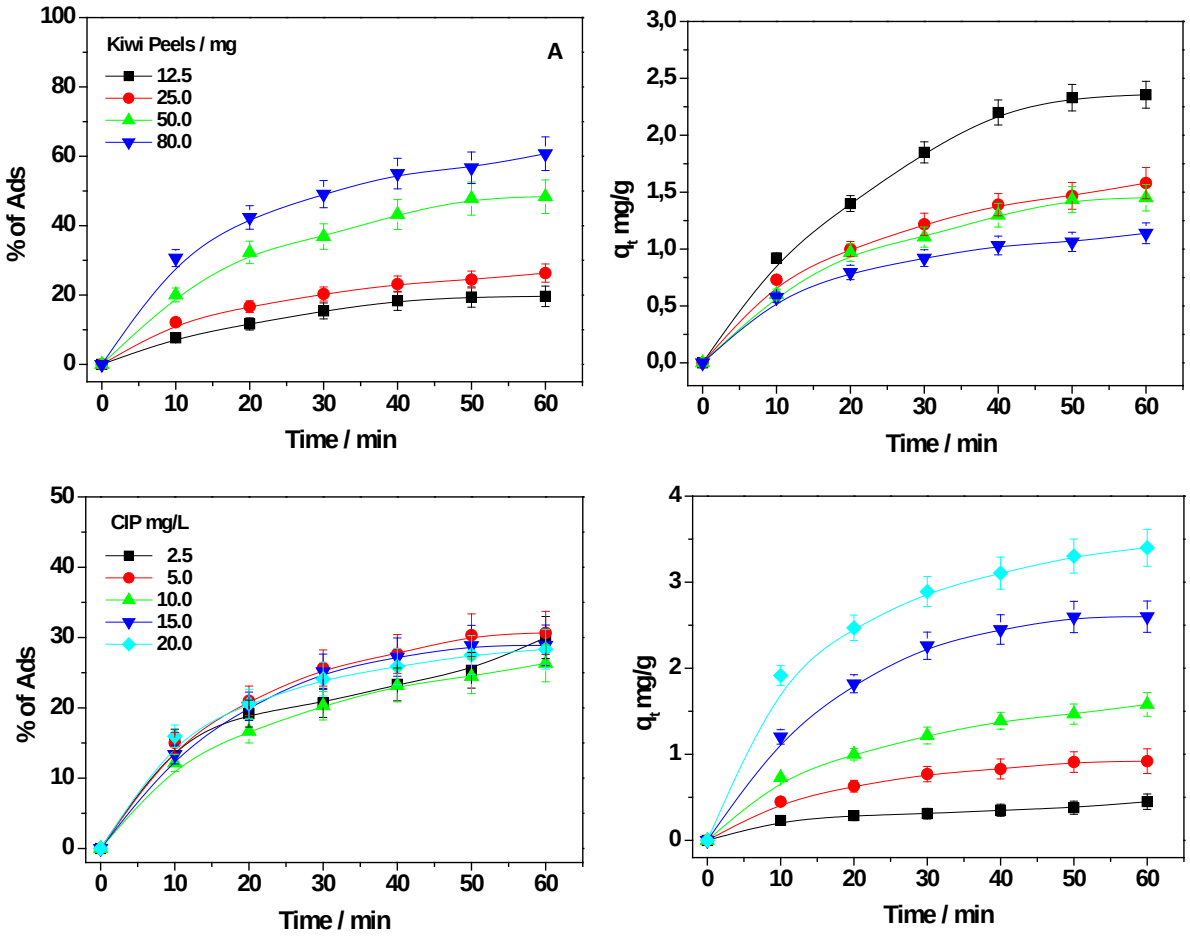

1189

1190 **Figure 4**

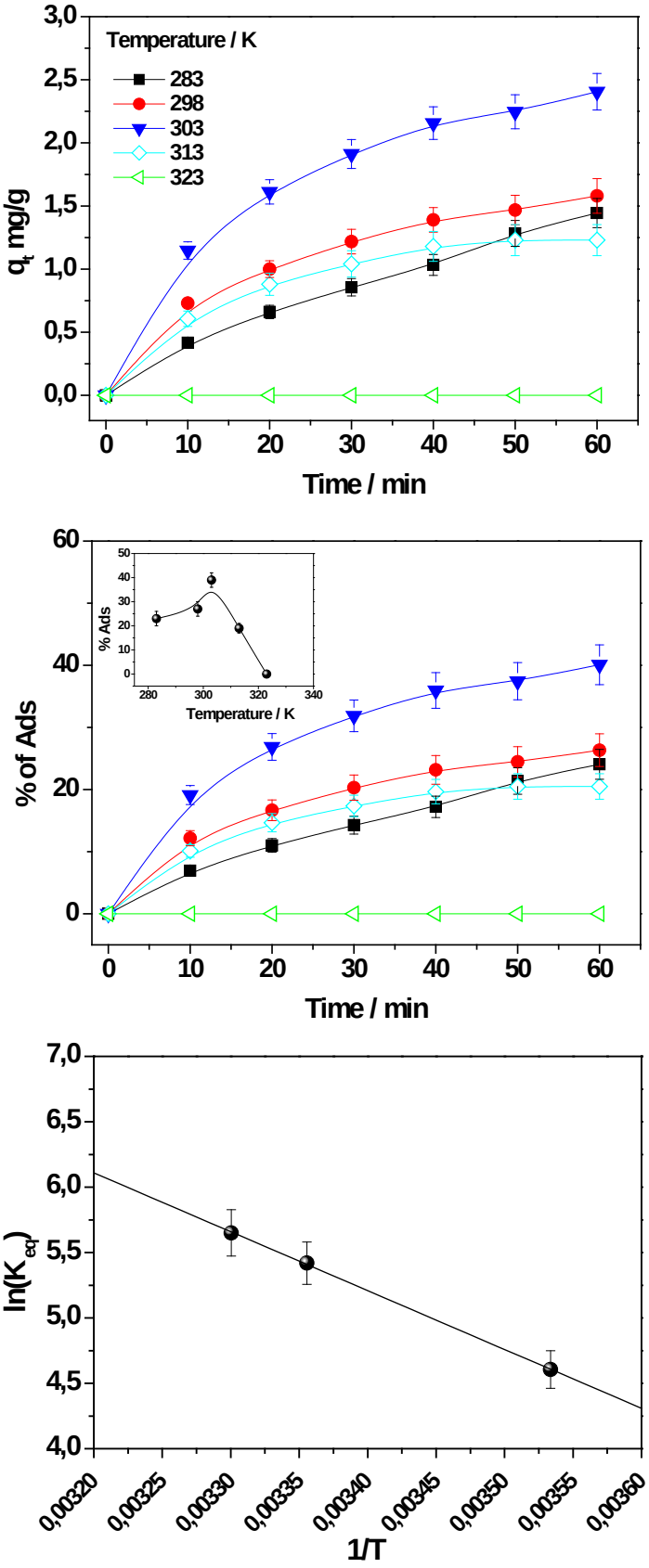

1191

1192 **Figure 5**

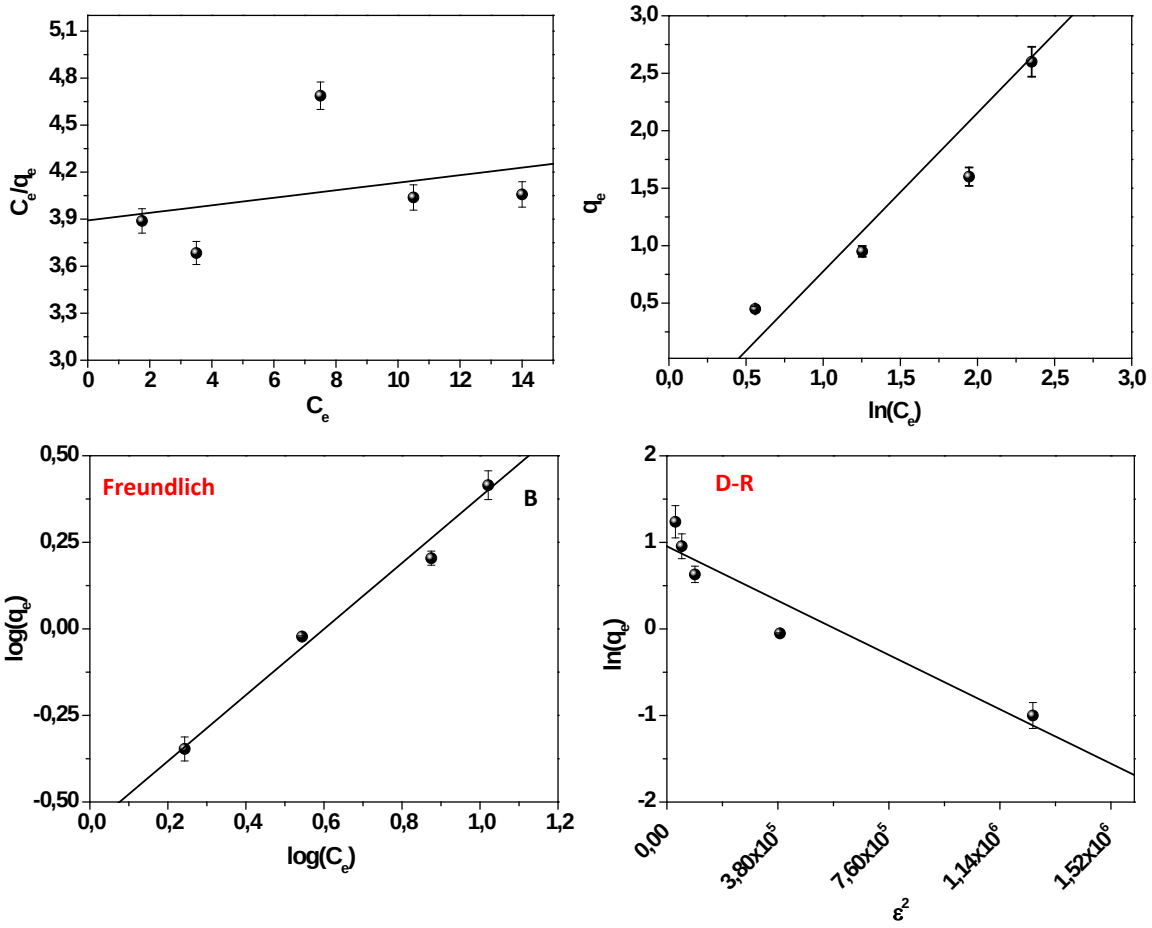

1193

1194 **Figure 6**

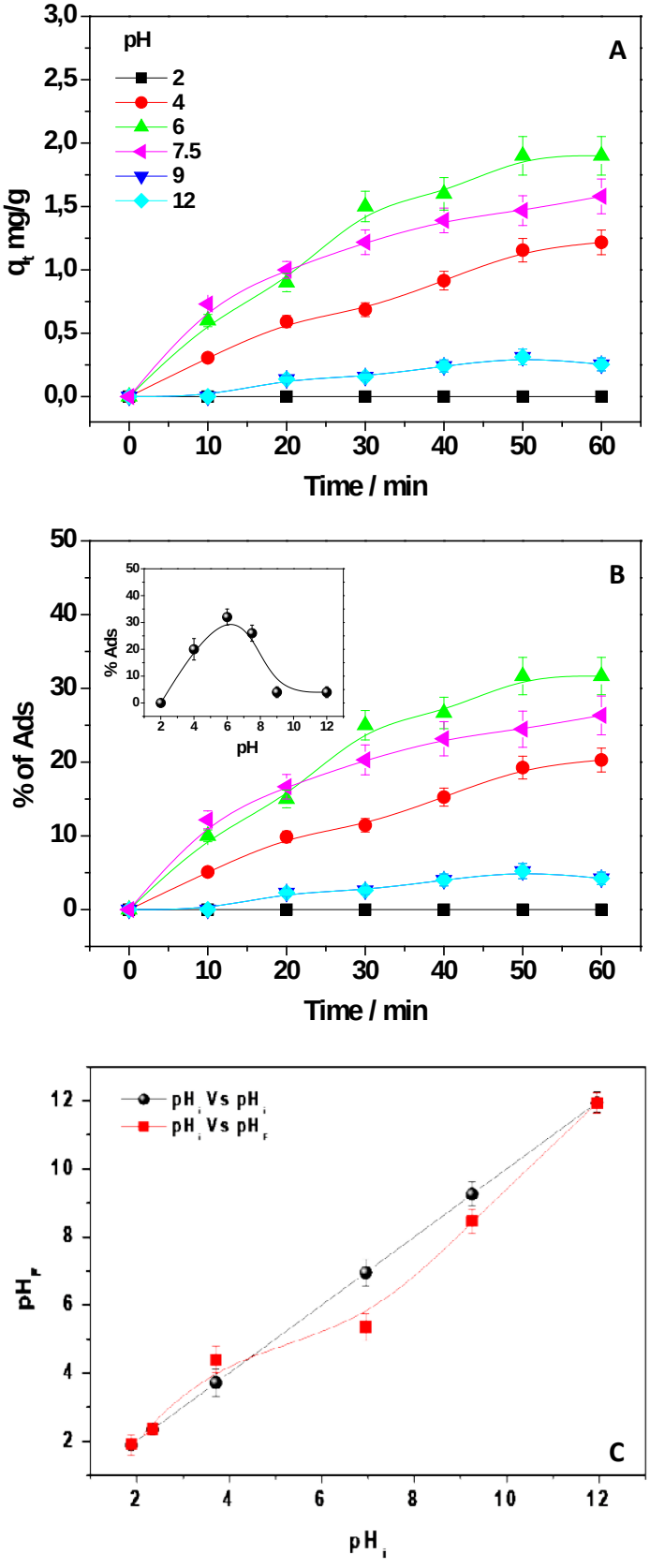

1195

1196 **Figure 7**

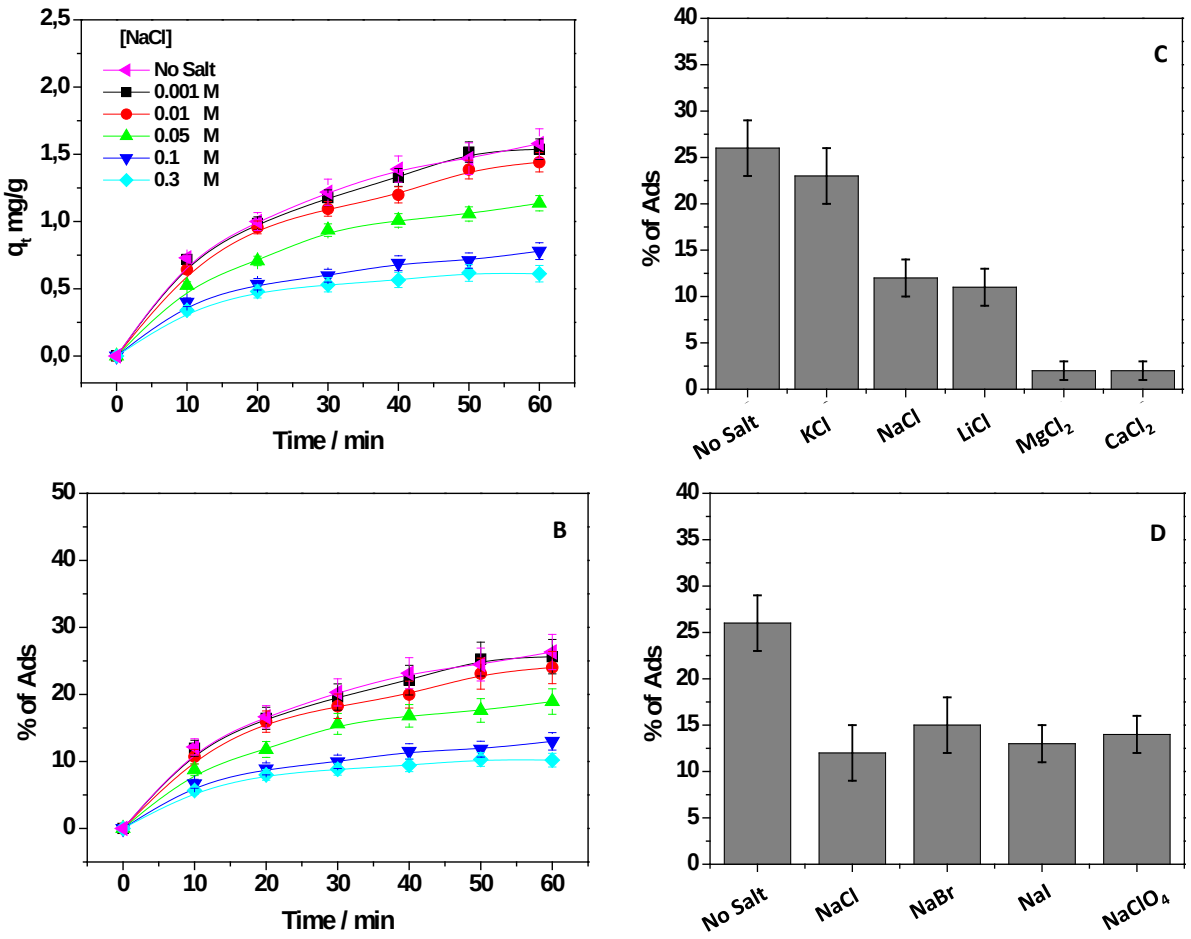

1197

1198 **Figure 8**

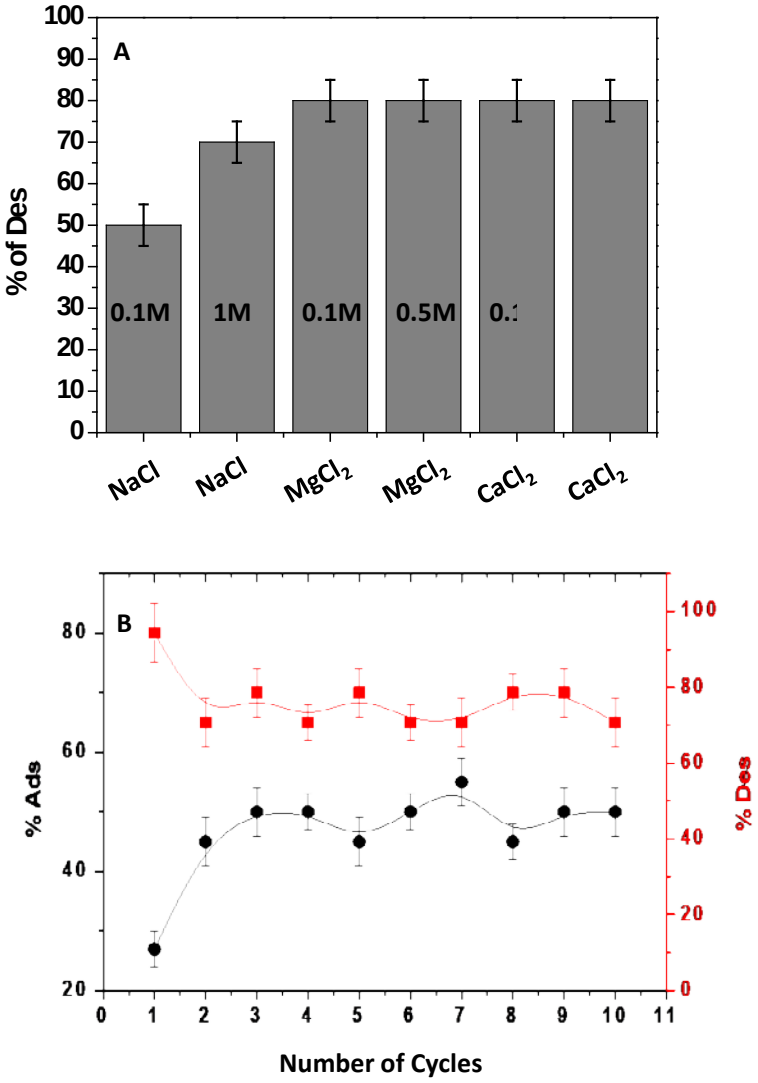

1199

1200 **Figure 9**

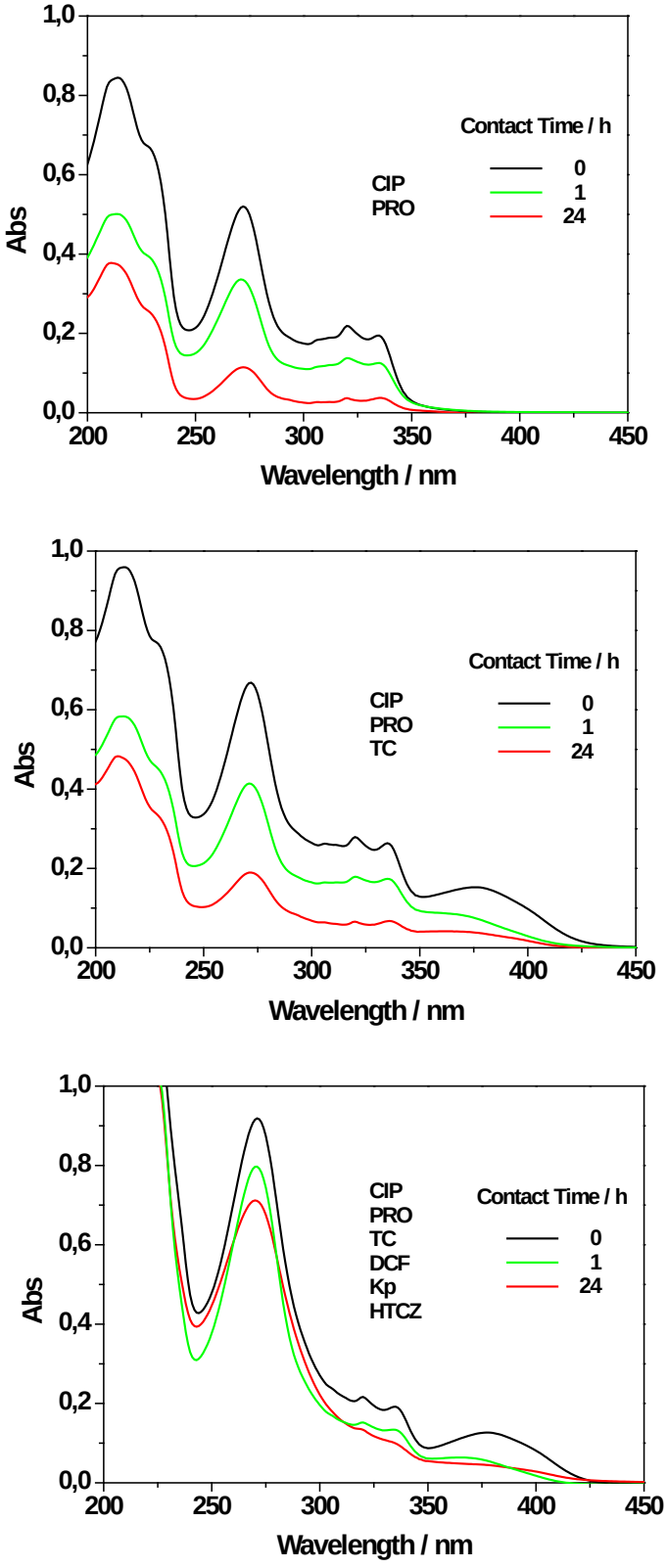

1201

1202 **Figure 10**

1203